Programa de doctorado
Dinámica de Flujos Biogeoquímicos y sus Aplicaciones

TESIS DOCTORAL

Integración de imágenes de sensores remotos en el desarrollo de indicadores medioambientales en cuencas mediterráneas. Aplicación al seguimiento de su estado hídrico y productividad

Integration of remote sensing images in the development of environmental indicators in Mediterranean basins. Application for monitoring water status and productivity

Doctorando:
Pedro Jesús Gómez Giráldez

Directores:
Dra María Patrocinio González Dugo
Dra Cristina Aguilar Porro

Febrero 2020

TITULO: *Integración de imágenes de sensores remotos en el desarrollo de indicadores medioambientales en cuencas mediterráneas. Aplicación al seguimiento de su estado hídrico y productividad*

AUTOR: *Pedro Jesús Gómez Giráldez*

Campus de Rabanales
Ctra. Nacional IV, Km. 396 A
14071 Córdoba

https://www.uco.es/ucopress/index.php/es/
ucopress@uco.es

TÍTULO DE LA TESIS: Integración de imágenes de sensores remotos en el desarrollo de indicadores medioambientales en cuencas mediterráneas. Aplicación al seguimiento de su estado hídrico y productividad

DOCTORANDO: Pedro J. Gómez Giráldez

INFORME RAZONADO DE LAS DIRECTORAS DE LA TESIS
(se hará mención a la evolución y desarrollo de la tesis, así como a trabajos y publicaciones derivados de la misma).

María Cristina Aguilar Porro, Profesora Titular de la Universidad de Córdoba, y María Patrocinio González Dugo, Investigadora Titular del Instituto de Investigación y Formación Agraria y Pesquera de Andalucía, IFAPA, como directoras de la tesis doctoral del alumno del Programa de Doctorado "Dinámica de Flujos Biogeoquímicos y sus Aplicaciones" Pedro Jesús Gómez Giráldez.

INFORMAN

Que el doctorando ha cubierto los objetivos presentados en la tesis, generado indicadores de distintas variables ecosistémicas relacionadas con la productividad y el estado hídrico en sistemas característicos de la región mediterránea combinando imágenes provenientes de sensores remotos de diferentes resoluciones espaciales, espectrales y temporales, con registros puntuales procedentes de estaciones meteorológicas. Tras la tesis, y como conclusión de ésta, se han desarrollado tres indicadores estrechamente ligados entre sí: un indicador del estado hídrico del suelo al final de la estación seca a partir del estado de distintas cubiertas vegetales; un indicador de la productividad de los pastos naturales, principal sustento alimenticio de la ganadería extensiva, a partir de su estado y las condiciones climáticas del período de estudio; y, por último, un indicador del estado hídrico del suelo a partir del estado fenológico en el que se encuentra la cubierta de pasto natural.

Además, el doctorando ha demostrado una gran capacidad de trabajo, tanto autónomo como en equipo, y ha perfeccionado su conocimiento sobre herramientas de modelado de la producción primaria bruta, realizando numerosos trabajos de campo para la medida directa de la misma. Ha gestionado datos procedentes de sensores remotos diversos y ha obtenido resultados en ecosistemas complejos como son las dehesas típicas del sudeste de la Península Ibérica y la montaña mediterránea. En ambos casos, la variabilidad en cuanto a la presencia de distintos estratos vegetales y gradientes climáticos, determina la presencia de estrés hídrico variable a distintas

escalas temporales lo que supone un reto a la hora de analizar tendencias en estos ecosistemas. Su capacidad expositiva y de discusión de resultados ha quedado de manifiesto en todas las ocasiones en las que ha participado en foros científicos, por lo que consideramos queda acreditada su excelencia como investigador en formación.

Tres de los capítulos de este trabajo se han plasmado en publicaciones en revistas indexadas en el JCR (Q1), además de una aportación a un congreso indexado con revisión por pares lo que avala la calidad del trabajo realizado.

Las publicaciones concretas que derivan de esta tesis son:

Artículos:

1 Gómez-Giráldez, P.J., Pérez-Palazón, M.J., Polo, M.J., González-Dugo, M.P., (2020). **Monitoring grass phenology and hydrological dynamics of an oak-grass savanna ecosystem using Sentinel-2 and terrestrial photography**. Remote Sensing, 12, 600; doi:10.3390/rs12040600

2 Gómez-Giráldez, P.J., Aguilar, C., Caño, A.B., García-Moreno, A., González-Dugo, M.P., (2019).**Remote sensing estimation of net primary production as monitoring indicator of holm oak savanna management.** Ecological Indicators, 106, 105526. Doi: https://doi.org/10.1016/j.ecolind.2019.105526

3 Gómez-Giráldez, P.J., Carpintero, E., Ramos, M., Aguilar, C., González-Dugo, M.P. (2018). **Effect of the water stress on gross primary production modeling of a Mediterranean oak savanna ecosystem.** Proc. IAHS, 95, 1–7, 2018. Doi: https://doi.org/10.5194/piahs-95-1-2018.

4 Gómez-Giráldez, P.J., Aguilar, C., Polo, M.J., (2014). **Natural vegetation covers as indicators of the soil water content in a semiarid mountainous watershed.** Ecological Indicators 46. 524–535. doi: 10.1016/j.ecolind.2014.06.024

Congresos

- Gómez-Giráldez, P.J., Torralbo, P., Polo, M.J., González-Dugo, M.P. 2019. Seguimiento fenológico de la vegetación de dehesa a partir de imagen digital terrestre e imágenes Sentinel-2. 58ª Reunión científica de la Sociedad Española de Pastos. Servicios ecosistémicos de los sistemas pastorales. 8-11 de Abril de 2019. Sevilla, España.
- Gómez-Giráldez, P.J., Carpintero, E., González-Dugo, M.P. 2019. Evaluación del efecto del estrés hídrico en el cálculo de la producción primaria bruta (GPP) de los pastos de dehesa mediante sensores remotos. 58ª Reunión científica de la Sociedad Española de Pastos. Servicios ecosistémicos de los sistemas pastorales. 8-11 de Abril de 2019. Sevilla, España.
- González-Dugo, M.P., Gómez-Giráldez, P.J., Carpintero, E., Andreu, A., 2019. Monitoring of pasture net primary production and water stress using remote sensing in a holm oak savanna rangeland. The 13th Dahlia Grienlinger International Symposium. 4-6 de Marzo de 2019. Haifa, Israel.
- Gómez-Giráldez, P.J., Aguilar, C., García, A., Caño, A.B., González-Dugo, M.P., 2018. Estimación de la producción de pastos herbáceos a diferentes escalas mediante sensores remotos. 57ª Reunión científica de la Sociedad

Española de Pastos. III Congreso Nacional de Vías Pecuarias y Trashumancia. 25-29 de Junio de 2018. Teruel, España.

- Gómez-Giráldez, P.J., Aguilar, C., García, A., Caño, A.B., González-Dugo, M.P., 2018. Estimation of pasture production at different scales using remote sensing in a holm oak savanna rangeland. Geophysical Research Abstracts, Vol. 20, EGU2018-14655, 2018. EGU General Assembly 2018. Vienna, Austria.
- Workshop: Current issues in hydrological sciences: scientific and societal challenges for the future. Universidad de Córdoba. (Octubre de 2017). Córdoba, España.
- Gómez-Giráldez, P.J., Aguilar, C., García-Moreno, A., Caño, A.B., González-Dugo, M.P., 2015. Estimación de la producción de pasto natural a partir de sensores remotos como apoyo a la gestión integral de ecosistemas de dehesa. Teledetección, humedales y espacios protegidos. XVI Congreso de la AET. 21-23 Octubre 2015. Sevilla, España.
- Workshop: Recent Advances in Snow Processes in Mediterranean Regions. Universidad de Córdoba. (Diciembre 2014). Córdoba, Spain
- Gómez-Giráldez, P.J., Jiménez, V., González-Dugo, M.P., 2014 Monitoring Pasture Production in Extensive Systems for an Integrated Management of Oak Savannas. Copernicus Users & Training Event, 13th - 14th February, Lisbon, Portugal.

Por todo ello, se autoriza la presentación de la tesis doctoral

Córdoba, 13 de febrero de 2020

Firma de las directoras

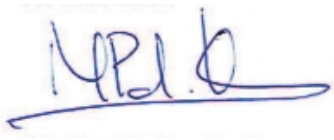

Fdo.:María Cristina Aguilar Porro

Fdo.: M.ª Patrocinio González Dugo

Tesis por compendio de artículos

Esta tesis cumple el requisito establecido por la Universidad de Córdoba para su presentación por compendio de artículos, con 3 artículos publicados en revistas incluidas en los 3 primeros cuartiles de la relación de revistas del ámbito de la especialidad.

1. Gómez-Giráldez, P.J., Aguilar, C., Polo, M.J., (2014). **Natural vegetation covers as indicators of the soil water content in a semiarid mountainous watershed.** Ecological Indicators 46. 524–535. doi: 10.1016/j.ecolind.2014.06.024

Datos de 2014 (JCR): índice de impacto 3.444, posición 34/223 (Q1) del área temática *Environmental sciences*.

2. Gómez-Giráldez, P.J., Aguilar, C., Caño, A.B., García-Moreno, A., González-Dugo, M.P., (2019).**Remote sensing estimation of net primary production as monitoring indicator of holm oak savanna management.** Ecological Indicators, 106, 105526. Doi: https://doi.org/10.1016/j.ecolind.2019.105526

Datos de 2018 (JCR): índice de impacto 4.49, posición 45/251 (Q1) del área temática *Environmental sciences*.

3. Gómez-Giráldez, P.J., Pérez-Palazón, M.J., Polo, M.J., González-Dugo, M.P., (2020). **Monitoring grass phenology and hydrological dynamics of an oak-grass savanna ecosystem using Sentinel-2 and terrestrial photography**. Remote Sensing, 12, 600; doi:10.3390/rs12040600

Datos de 2018 (JCR): índice de impacto 4.118, posición 7/30 (Q1) del área temática *Remote Sensing*.

El doctorando:

Fdo: Pedro J. Gómez Giráldez

La ciencia es el poder del ser humano
(Gendo Rokubungi, Neon Génesis Evangelion)

AGRADECIMIENTOS

A mis directoras, Mª Pat y Cristina, sin su confianza esto no hubiera sido posible.

A los compañeros del Máster de Hidráulica Ambiental porque ahí empezó la motivación.

A los compañeros de DFH, gracias al equipo montado por María José aprendí a ser investigador. Mención especial a Elena y Pepa que me han sacado de más de un apuro.

A mis compañeros de IFAPA, Alma, Belén, Ana, Eli, Mario… una parte de esta tesis también es vuestra.

Al apoyo externo de mis amigos que me han hecho todo más fácil y me han tenido que soportar. En especial a David y Truji porque siempre me han dado buenas soluciones en momentos críticos, y a Manolo por su ayuda artística.

A mis hermanos, que da igual lo que haga que siempre me apoyarán.

A Pao (y Finidi) porque ha conseguido que el tramo final sea más llevadero, gracias.

Y, por supuesto, a mis padres, a los que se lo debo todo.

Índice

RESUMEN

En las cuencas mediterráneas, el clima se caracteriza por veranos muy calurosos en los que no se suelen producir precipitaciones, lo que genera un fuerte y periódico estrés hídrico en sus cubiertas vegetales cuya intensidad está relacionada con el carácter hidrológico de la estación húmeda antecedente. Además, esta situación tiende a agravarse en los frecuentes episodios de sequía, provocando una disminución de la productividad de estos ecosistemas. Actualmente existe una gran cantidad de datos disponibles, gratuitos y a escala global, con un gran potencial para el seguimiento de los procesos asociados a los balances de agua y energía en estos tipos de cuencas.

En esta tesis se plantea el uso de imágenes provenientes de sensores remotos de diferentes resoluciones espaciales, espectrales y temporales que, combinadas con registros puntuales procedentes de estaciones meteorológicas, permitan la generación de indicadores de distintas variables ecosistémicas relacionadas con la productividad y el estado hídrico en sistemas característicos de la zona mediterránea. En concreto, se plantea el desarrollo de tres indicadores estrechamente ligados entre sí: un indicador del estado hídrico del suelo al final de la estación seca a partir del estado de varios tipos de cubierta vegetal; un indicador de la productividad de los pastos naturales, principal sustento alimenticio de la ganadería extensiva, a partir de su estado y de las condiciones climáticas del período evaluado; y, por último, un indicador que relacione el estado hídrico del sistema y el estado fenológico en el que se encuentra el estrato herbáceo. Las zonas de estudio seleccionadas son, para el primer indicador, la cuenca del río Guadalfeo (Granada), que se caracteriza por presentar un gradiente de altitud desde el nivel del mar hasta más de 3000 m.s.n.m. a tan solo 50 km de distancia a la costa, lo que determina una gran heterogeneidad espacial en cuanto a meteorología, hidrología, tipos y usos de suelo, etc. En este contexto, la estimación indirecta del estado de humedad antecedente de forma rutinaria a partir de la información obtenida de ciertas cubiertas existentes en la zona puede ser una solución óptima en estudios hidrológicos a escala de cuenca. En cuanto al segundo y tercer indicador, la zona de estudio son los ecosistemas de dehesa de Andalucía. El seguimiento regular y de forma objetiva de la producción de pasto permitiría proporcionar a los propietarios y gestores una información clave para regular su uso y contribuir a su conservación, sin un aumento excesivo de los costes. Por otro lado, los cambios fenológicos que se pueden observar como consecuencia del calentamiento global, cuyo efecto se prevé especialmente intenso en esta región, y cómo el clima y la hidrología los condicionan, puede ser una herramienta clave para evaluar el impacto de esta amenaza y tomar las decisiones adecuadas para hacerle frente.

Los resultados han mostrado la capacidad de los sensores remotos para la obtención de este tipo de indicadores: el contenido de agua en el suelo en época estival presentó correlaciones mayores a 0,7 con el estado de la vegetación arbustiva de la cuenca del Guadalfeo; la estimación de la producción de pasto natural en las dehesas de Andalucía arrojó errores en torno al 13% con respecto a la producción medida en campo; por último, los umbrales de cambio de estado en la humedad de suelo (capacidad de campo y punto de marchitez permanente) se determinaron con menos de 10 días de diferencia con respecto a los cambios de estado fenológico en el pasto natural (comienzo de la época de crecimiento y senescencia).

ABSTRACT

In the Mediterranean basins, the climate is characterized by very hot summers in which rainfall is not usually produced, which generates a strong and periodic water stress in its vegetation cover. The intensity of this water stress is related to the hydrological regime of the previous wet season. In addition, this situation tends to worsen in frequent episodes of drought, causing a decrease in the productivity of these ecosystems. There is currently a large amount of data available, free of charge and on a global scale, with great potential for monitoring the processes associated with water and energy balances in these types of basins.

This thesis proposes the use of remote sensing images of different spatial, spectral and temporal resolutions that, combined with specific records from meteorological stations, can be used to generate indicators of different ecosystem variables related to productivity and water status in different unique systems of the Mediterranean area. Specifically, the development of three indicators closely linked to each other is proposed: an indicator of the water status of the soil at the end of the dry season from the state of different vegetation covers; an indicator of the productivity of natural pastures, the main food support for extensive livestock, based on their status and the climatic conditions of the period evaluated; and, finally, an indicator of the relationship bewteen water state of the soil and the natural pasture phenological state. The selected study areas are, for the first indicator, the Guadalfeo river basin (Granada), characterized by presenting a gradient of altitude from sea level to more than 3000 m.a.s.l. only 50 km away from the coast, which determines a great spatial heterogeneity in terms of meteorology, hydrology, types and land soil, etc. In this context, the indirect estimation of the state of antecedent moisture from the information obtained from existing covers in the area may be an optimal solution in hydrological studies at basin scale. Regarding the second and third indicators, the study area is the dehesa ecosystems of Andalusia, since the monitoring of pasture production would provide key information to owners and managers to regulate their use and contribute to their conservation, without an excessive increase in costs. On the other hand, the phenological changes that can be observed as a result of global warming, whose effect is expected to be especially intense in this region, and how the climate and hydrology condition them, can be a key tool to assess the impact of this threat and make the right decisions to deal with it.

The results have shown the ability of remote sensing to obtain this type of indicators: the water content in the soil during the summer season showed correlations greater than 0.7 with the state of shrub vegetation; the estimation of the production of natural pastures showed errors of about 13% with respect to the production measured in the field; finally, the thresholds of change of state in soil moisture (field capacity and permanent wilting point) were determined less than 10

days apart from changes in phenological state in natural grass (beginning of time of growth and senescence).

CAPÍTULO I
INTRODUCCIÓN GENERAL Y OBJETIVOS

I.1. Características climáticas e hidrológicas de las cuencas mediterráneas

Las zonas que presentan clima mediterráneo se encuentran entre los 30º y 45º de latitud (Aschmann, 1973) y aunque la mayor parte se encuentre concentrada en el mar Mediterráneo, cubriendo un 20% de la superficie de la Unión Europea, también se extiende por las costas de California, Chile, Sudáfrica y el sur de Australia (Strahler y Strahler, 1989). Este clima se caracteriza principalmente por su estacionalidad (Martín Vide y Olcina, 2001), presentando inviernos suaves y húmedos y veranos secos y calurosos. La temperatura media anual está en torno a los 16,5 ºC pero la amplitud térmica es bastante grande al presentar valores sobre los 40ºC en verano y bajo cero en invierno. La precipitación media anual es de unos 600-650 mm pero varía mucho desde las zonas más áridas con menos de 300 mm, a las más húmedas con unos 1000 mm. Esta variabilidad se debe a la cercanía o lejanía al mar y al incremento de ésta con la altitud (Robles et al., 2002). Por lo general, en zonas de interior nos encontramos un ambiente más frío y seco, y en cotas altas hay un régimen mayor de precipitaciones. Una particularidad del régimen de precipitaciones es que la ocurrencia de las mismas no tiene lugar en verano, lo que, unido a que en esta época se da el máximo en temperaturas, produce un importante estrés hídrico que da lugar a periodos de fuertes sequías y posteriores eventos de torrencialidad una vez se producen las primeras lluvias (Molina et al., 1994). Esto hace al clima mediterráneo especialmente vulnerable al cambio climático (Kovats et al., 2014), donde las proyecciones actuales para esta región prevén un aumento de la temperatura y un mayor cambio en el régimen de precipitaciones (Norant y Douguédroit, 2006; Cortesi et al., 2007; Solomon et al., 2017).

En esta tesis se ha querido recoger la variabilidad climática de los ecosistemas mediterráneos seleccionando dos sistemas que cubren gran parte del territorio de la Comunidad Autónoma de Andalucía: ecosistema de montaña mediterránea y ecosistema de dehesa (Fig I.1).

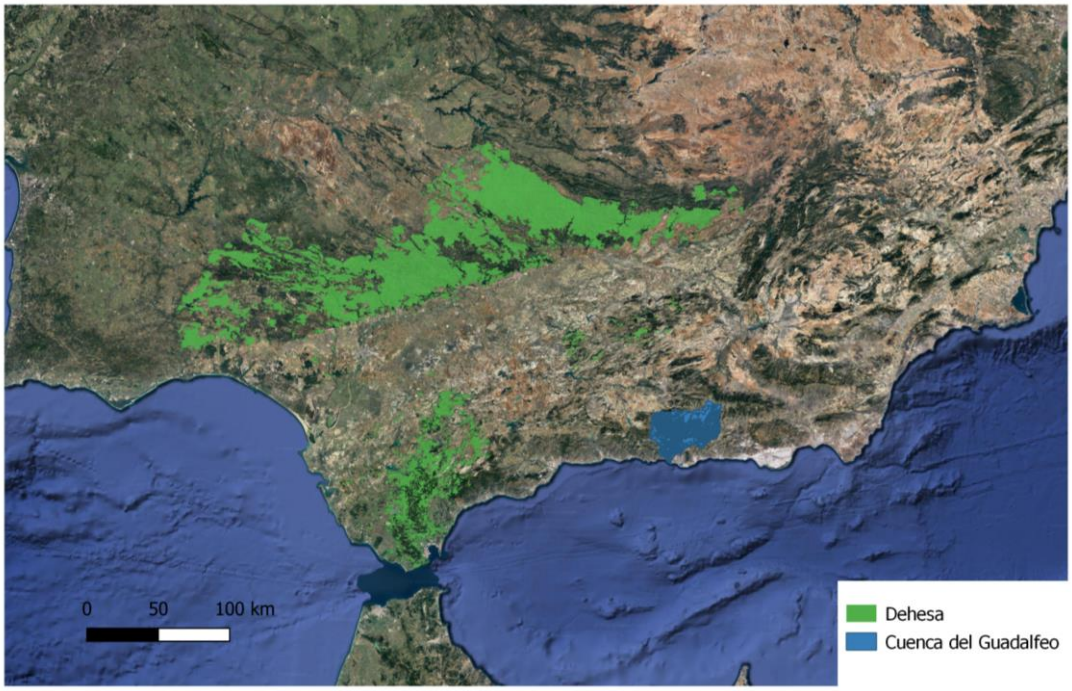

Figura I.1. Situación de las zonas de estudio de la tesis: zona de dehesa de Andalucía (verde) y cuenca del Guadalfeo (azul).

La zona escogida de representación de montaña mediterránea es la cuenca del río Guadalfeo (Granada), en la cual se pueden encontrar cinco de los seis pisos bioclimáticos existentes en el clima mediterráneo (Rivas-Martínez 1987) en apenas los 50 km que separan la costa de su máxima altitud de 3482 m.s.n.m. El termomediterráneo, con una importante influencia costera y con la casi total ausencia de heladas; el mesomediterráneo con heladas en invierno y sequía estival; el supramediterráneo, que corresponde a media montaña, presenta temperaturas muy bajas en el invierno, pero en el verano las temperaturas son más suaves que en el anterior; el oromediterráneo, que es el piso de alta montaña cubierto de nieve buena parte del invierno; y el crioromediterráneo que corresponde a las zonas de cumbres.

En cuanto al segundo ecosistema tipo analizado, las zonas de dehesa, se aborda el seguimiento de la totalidad de la zona de dehesa de Andalucía, que cubre más de un millón de ha ($1.07 \cdot 10^6$ ha, https://www.cma.junta-andalucia.es/medioambiente/site/rediam). Este ecosistema está presente tanto en zonas de montaña como en altitudes más bajas, teniendo la particularidad de haber sido conformadas por el ser humano para su aprovechamiento. La gran extensión abarcada conlleva una amplia variabilidad en las mismas en cuanto a características de precipitación y temperaturas.

I.2. Características de las cubiertas vegetales en cuencas mediterráneas

La vegetación mediterránea está constituida preferentemente por especies perinnifolias de hojas pequeñas y coriáceas (Almeida, 2009) y bosques de no mucha densidad arbórea pero sí un denso sotobosque como consecuencia del clima cálido y seco. En zonas de poca altitud predominan los *Quercus spp*, mientras que en zonas más altas comienzan a aparecer coníferas principalmente *Pinus spp*, y *Abies spp*. El sotobosque está formado por una gran diversidad de matorral, tanto en especies como en estructura, y por pastizales. Esta diversidad da lugar a un gran número de endemismos y especies protegidas. En concreto en las zonas mediterráneas se pueden encontrar 146 tipos de hábitats, 148 especies animales y 270 especies de plantas de interés comunitario (Red Natura 2000). Gran parte de esta vegetación queda representada en las zonas de estudio seleccionadas en este trabajo.

Parte de la cuenca del Guadalfeo se encuentra dentro del Parque Natural y Nacional de Sierra Nevada, contando con especies endémicas como como son *Artemisa granatensis*, *Areanria pungens*, *Dianthus brachyabnthus* o *Alyssum longicaule*. En esta cuenca, debido a su fuerte gradiente altitudinal y al igual que se encuentran distintos pisos bioclimáticos, se extienden amplias zonas de matorrales típicos mediterráneos que se mezclan a veces con masas poco densas de *Quercus spp* y zonas de pinares de repoblación. En las zonas más altas se encuentra pastizal de alta montaña.

Las zonas de dehesa estudiadas están fundamentalmente compuestas por pastizales con un estrato arbóreo de *Quercus ilex* y *Quercus suber* (este último más predominante en la mitad occidental de Andalucía). Los pastos de la dehesa constituyen formaciones vegetales con una elevada diversidad, hasta 164 especies vegetales en una finca (proyecto BIOBIO). La amplia distribución de la dehesa y la variabilidad climática que esta distribución conlleva, unida a la propia gestión de estas fincas (métodos de pastoreo y paisajes en mosaico) hacen posible esta biodiversidad (García-Moreno et al., 2016). En este ecosistema, además de la intervención humana, la disponibilidad de agua es fundamental en la conformación de un paisaje combinado de pastos y árboles, que es el único estado estable de equilibrio cuando ocurre una marcada estacionalidad en la disponibilidad de agua (Eagleson y Segarra, 1985). Además de su importancia en la biodiversidad, los pastos de dehesa son el principal alimento de la ganadería extensiva propia de estos sistemas, lo que los convierten en un recurso económico fundamental cuyo adecuado mantenimiento requiere la continua intervención humana. Por ello, la estimación de su producción es útil para el seguimiento del estado de la vegetación y puede informar sobre la idoneidad/insuficiencia de su gestión.

La variabilidad climática descrita anteriormente propia de la cuenca mediterránea junto a la cambiante topografía de las regiones concretas de estudio (donde se alternan zonas rocosas,

montañosas, altitudes medias, zonas de playa, etc.) tienen un importante efecto en la variedad de asociaciones vegetales y por tanto en su biodiversidad, ya que la vegetación que crece en un área determinada establece relaciones de interacción entre sí formando asociaciones vegetales características. Además, se han observado cambios fenológicos como resultado de cambios en el clima (Nazir et al., 2018), por lo que el seguimiento de la fenología de estos ecosistemas mediterráneos es clave para evaluar adecuadamente los impactos del calentamiento global. Este seguimiento requiere observaciones frecuentes y que requieren mucho tiempo y recursos, especialmente en áreas de difícil acceso..

I.3. Sensores remotos: funcionamiento y características

El término “sensores remotos” hace referencia a aquellos instrumentos que pueden captar información de un objeto a cierta distancia. En el ámbito de la observación de la tierra, esta información se presenta en forma de imágenes de la superficie terrestre obtenidas por sensores instalados generalmente en plataformas aéreas o espaciales. Esta obtención remota de imágenes junto a las técnicas de análisis de las mismas es lo que se conoce como teledetección (Chuvieco 1990). Este tipo de observaciones se remontan a las fotografías obtenidas desde globos aerostáticos en el siglo XIX, pero la primera cámara aérea se usó en la Primera Guerra Mundial donde quedó patente la utilidad estratégica de estas técnicas (Brookes, 1975) que ya se desarrollaron ampliamente en la Segunda Guerra Mundial. No fue hasta 1960 cuando comenzó el uso civil de la teledetección (TIROS-1, satélite para observación meteorológica) y hoy en día es ampliamente utilizada en campos como la cartografía, agricultura, valoración ambiental, arqueología o seguimiento de catástrofes (Baker et al., 2001). Esta expansión se debe a las ventajas que presenta esta técnica, como permitir una cobertura global cuando se emplean satélites, la posibilidad de análisis multiescala no destructivos, proporcionar información en regiones no visibles del espectro, o la repetitividad e inmediatez en formato digital (Chuvieco 2002).

La teledetección puede emplear dos tipos de sensores: activos o pasivos. Los sensores activos emiten energía y posteriormente registran la radiación reflejada por el objetivo (por ejemplo, los sistemas de radar), mientras que los pasivos detectan la radiancia natural emitida o reflejada por objetivo como respuesta a la radiación solar incidente. En cualquiera de los casos, el flujo de energía entre la superficie objetivo y el sensor constituye una radiación electromagnética. Esta radiación se agrupa en distintas regiones con longitudes de onda (o frecuencia) con un comportamiento similar que se denomina espectro electromagnético (Fig I.2). En esta tesis se utilizan únicamente sensores pasivos y se presta especial interés a las regiones del visible (VIS) y del infrarrojo cercano (NIR), regiones en las cuales la vegetación presenta comportamientos característicos en función de su abundancia, estado o vigor.

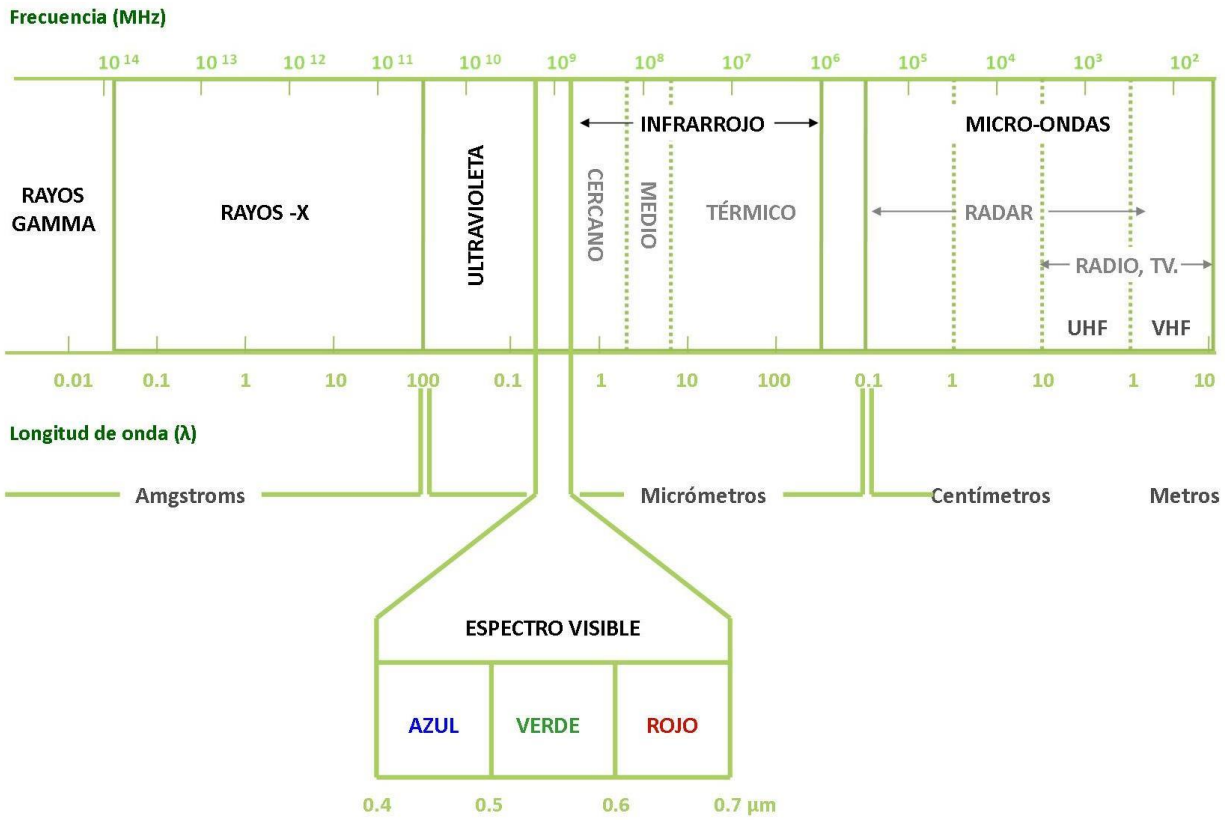

Figura I.2. Espectro electromagnético. Fuente: Elaboración propia a partir de Chuvieco 1990.

Las propiedades de las imágenes proporcionadas por cada sensor dependen de la combinación de resoluciones que posea el sistema: (i) resolución espacial o tamaño en tierra del píxel de la imagen, (ii) espectral o número de bandas, longitud de onda y anchura que mide el sensor en el espectro electromagnético,(iii) radiométrica o capacidad del sensor para distinguir diferentes intensidades de radiación y (iv) temporal o frecuencia de adquisición de imágenes sobre un mismo punto. Estas resoluciones a menudo están relacionadas entre sí a la hora de escoger un sensor u otro en función del objetivo del estudio, puesto que el aumento de cualquiera de las cuatro resoluciones implica un aumento del volumen de datos. En esta tesis se han usado imágenes provenientes de los siguientes sensores a bordo de satélites (ordenados de menor a mayor resolución espacial):

- MODIS (Moderate Resolution Imaging Spectroradiometer): a bordo de los satélites Aqua y Terra posee una resolución temporal de 1 a 2 días, una resolución espectral de 36 bandas que van desde 0.4 a 14 µm, una resolución radiométrica de 12 bits y una resolución espacial de 250 m (bandas 1 y 2), 500 m (bandas 3 a 7), 1 km (bandas 8 a 36) (https://modis.gsfc.nasa.gov/about/specifications.php).

- TM (Thematic Mapper) y ETM+(Enhanced Thematic Mapper Plus): a bordo de los satélites Landsat 5 y Landsat 7 respectivamente. Ambos sensores presentan una resolución temporal de

16 días, una resolución espectral de 7 bandas TM y de 8 ETM+ que van de 0.45 a 12.5 µm, una resolución radiométrica de 8 bits y una resolución espacial de 30 m (bandas de 1 a 5 y 7). Ambos sensores presentan una banda 6 en la región del térmico con una resolución espacial de 120 m para TM y de 60 m para ETM+. Además, ETM+ posee una banda pancromática (banda 8) de 15 m de resolución espacial (https://landsat.gsfc.nasa.gov/the-thematic-mapper/; https://landsat.gsfc.nasa.gov/the-enhanced-thematic-mapper-plus/).

- MSI (MultiSpectral Instrument): a bordo de los satélites Sentinel-2 (A y B) presentan una resolución temporal de 10 días (5 días si se combinan Sentinel-2A y Sentinel-2B), una resolución espectral de 13 bandas de 0.44 a 22 µm, una resolución radiométrica de 12 bits y una resolución espacial de 10 m (bandas 2 a 4 y 8), 20 m (bandas 5 a 7, 8a, 11 y 12) y 60 m (bandas 1, 9 y 10) (https://sentinel.esa.int/web/sentinel/user-guides/sentinel-2-msi/resolutions).

El uso combinado de información procedente de este grupo de sensores permite hacer un estudio en detalle de las zonas mediterráneas a diferentes escalas espaciales, abordando la escala regional (MODIS), la escala de cuenca (TM y ETM+) y la escala de parcela (MSI). La selección de la escala espacial idónea para cada estudio concreto condiciona el éxito de este pues las relaciones entre variables ambientales pueden variar al modificarse la escala (Andersson et al., 2011; Ehlerinder y Field, 1993).

I.4. Aplicación de sensores remotos a las cubiertas vegetales

La radiancia que captan los sensores remotos pasivos en las distintas regiones del espectro electromagnético es función de la cantidad de radiación que reflejan las distintas cubiertas terrestres en dichas longitudes de onda. La radiación reflejada por cada superficie es lo que se conoce como reflectividad, y si se expresa en función de la longitud de onda se conoce como firma espectral. La Fig I.3 muestra un ejemplo de la firma espectral de pasto natural y de suelo desnudo en la región VIS/NIR/SWIR, medida en campo con un radiómetro de campo ASD FieldSpec en una finca de dehesa en Cardeña (Córdoba) en febrero de 2019. En ella se puede observar cómo la reflectividad del suelo desnudo aumenta ligeramente y de forma más o menos constante de las bandas visibles a la infrarroja del espectro. Por el contrario, el pasto muestra una reducida reflectividad en las bandas visibles, con una ligera subida en el verde (550 nm aproximadamente), y con un fuerte incremento en el infrarrojo cercano.

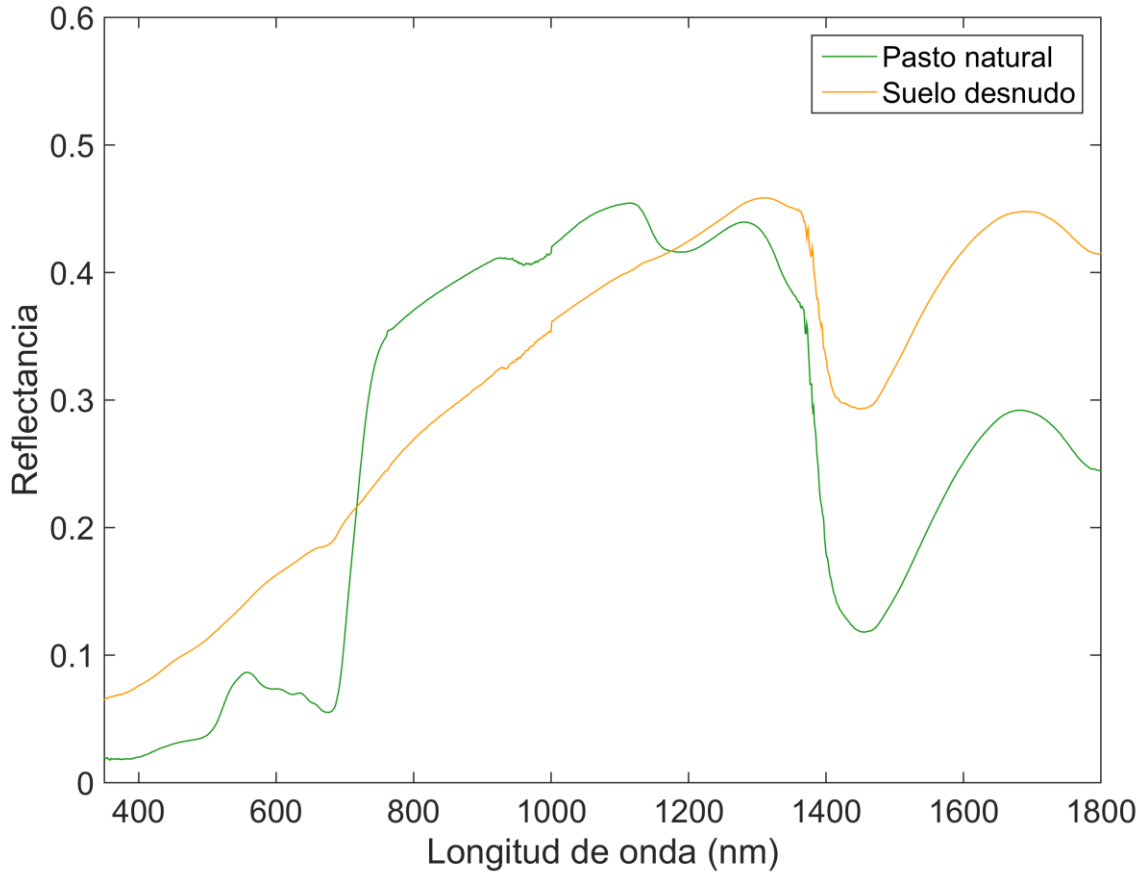

Fig I.3. Firma espectral de pasto natural y de suelo desnudo tomadas con un radiómetro de campo ASD FieldSpec en una finca de dehesa en Cardeña (Córdoba) en febrero de 2019.

A su vez, cada cubierta concreta presenta variaciones en su respuesta espectral respecto a las curvas promedio en función de diversos factores. En el caso de la vegetación, tanto su composición química (contenido de clorofila, nitrógeno, fibra, etc..) como el contenido de humedad del mesofilo o la estructura de la cubierta modifican la reflectividad en diferentes porciones del espectro. En el caso del suelo, su contenido en humedad y el color, derivado de su composición, son los factores más influyentes. Por ello, el análisis de las variaciones del espectro en un suelo concreto permite, por ejemplo, obtener información sobre la evolución del contenido de humedad de este. No obstante, estos datos son solo representativos de los primeros centímetros del perfil del suelo (Ellis et al., 2009) no cubriendo muchos procesos hidrológicos que puedan ser de interés.

El comportamiento espectral de las cubiertas vegetales es la base sobre la que se desarrollaron los índices de vegetación, que son una combinación algebraica de los valores de reflectividad medidos en diferentes bandas. Están diseñados para extraer la máxima información

relacionada con la vegetación, minimizando la influencia de perturbaciones como las debidas al suelo y a las condiciones atmosféricas (Huete, 1988).

Los índices de vegetación han sido usados de manera efectiva en múltiples aplicaciones, como se muestran diversas revisiones sobre el tema en los últimos años (Glenn et al 2008; Xue y Su 2017). Entre estas aplicaciones está la caracterizarización cultivos y cubiertas naturales a través el seguimiento de diferentes variables biofísicas como la fracción de cobertura, el índice de área foliar, o la fracción de PAR (Radiación fotosintéticamente activa) absorbida (Padilla et al 2011; González-Dugo & Mateos, 2008). Estas variables son empleadas con frecuencia como información de partida para modelar los intercambios de agua (González-Dugo et al. 2009, Jódar, et al. 2018), energía (Andreu et al., 2015, 2018) y CO_2 (Klosterhalfen et al., 2019; Huete et al., 2015) entre la cubierta terrestres y la atmósfera. Estos últimos han sido aplicados con éxito sobre bosques homogéneos (Zhou et al., 2017), pastizales abiertos (Hill et al., 2004) o cultivos (Yuan et al., 2015). Sin embargo, la mayor parte de las aplicaciones se centran en ecosistemas completos y homogéneos, prestando escasa atención al comportamiento diferente de los componentes específicos del dosel.

El seguimiento de la climatología/hidrología en los climas mediterráneos se hace difícil ya que las variables necesarias para su calibración (Chaponnière et al., 2008) suelen requerir estaciones de aforo que muchas veces distan demasiado de la zona de estudio en particular. Además, la ausencia de precipitaciones en el periodo estival hace imposible evaluar el estado hidrológico de las cuencas mediterráneas en esta época (Maneta et al., 2008) y están determinados en gran medida por las condiciones previas de humedad del suelo (Castillo et al., 2003). Por ello, la calibración de modelos hidrológicos constituye un problema importante en áreas semiáridas. En este contexto, el estado de la vegetación derivado de los índices de vegetación ha servido como herramienta indirecta para estimar cambios en la disponibilidad de agua (Aguilar et al 2012) o como indicador del régimen global anual (Gómez-Giráldez et al 2012)

Por otro lado, los sensores remotos abren nuevas posibilidades para complementar aproximaciones para caracterizar la dinámica de la vegetación que tradicionalmente han requerido un intenso trabajo de campo, como es el seguimiento fenológico. Este interés se ha intensificado además en los últimos años debido al impacto del cambio climático en los cambios fenológicos de las plantas. Ejemplo de ello son los estudios que muestran seguimientos a escala global (Jin et al 2013), en cultivos (Peña-Barragán et al 2011, Poenaru et al 2017) o en bosques (Pastor-Guzmán et al 2018). El sensor MSI a bordo de Sentinel-2 se ha usado con éxito en seguimiento fenológico, sobre todo combinado con otros satélites (Skakun et al 2019) debido a la escasa serie temporal disponible ya que fue lanzado en 2015. Este sensor presenta nuevas posibilidades por poseer bandas en el *Red Edge*, la región de cambio rápido en la vegetación aproximadamente a 700 nm

(Fig I3), pero este potencial para mejorar la precisión de la estimación de las etapas de transición fenológica aún no se ha explorado por completo.

A pesar de las ventajas que ofrece la teledetección en el seguimiento de la fenología, como la posibilidad de abordar de forma simultánea grandes superficies o alcanzar zonas de difícil acceso, siempre es necesario complementar esta información con medidas en campo, en ocasiones difícil de conseguir. Con frecuencia estos datos no están disponibles por la dificultad de acceso, en otros casos su repetitividad no es suficiente para llevar a cabo estos estudios. En los últimos años, el uso de cámaras digitales terrestres ha empezado a representar una solución rentable en muchas aplicaciones de seguimiento fenológico. Estas cámaras proporcionan información confiable y en tiempo real para el seguimiento de la fenología de la vegetación y existen redes bien consolidadas para compartir estos datos como la red PHENOCAM (https://phenocam.sr.unh.edu/webcam/). El uso combinado de toda esta información tiene un importante valor para profundizar en el seguimiento de la fenología de las plantas y su relación con la dinámica hidrológica del ecosistema.

I.5. Objetivos

El objetivo general de esta tesis es evaluar el potencial de la información proporcionada por los sensores remotos para desarrollar indicadores medioambientales que permitan cuantificar y realizar un seguimiento objetivo y regular de la vegetación de las cuencas mediterráneas, prestando especial atención a su productividad y al estado hídrico del sistema. Para ello, se plantean los siguientes objetivos específicos:

- Caracterizar de las principales variables biofísicas que describen estos sistemas y su estado, y que pueden ser derivadas a partir de los datos proporcionados por sensores remotos.

- Evaluar el uso del estado de la vegetación natural en condiciones semiáridas, determinado mediante sensores remotos, como indicador del estado hídrico del suelo, y analizar su relación con las características hidrológicas antecedentes a escala de cuenca empleando para ello un modelo hidrológico distribuido.

- Desarrollar y evaluar el funcionamiento de un modelo de estimación de biomasa adaptado a los pastos de la dehesa y que tenga en consideración la existencia y el efecto del arbolado. Explorar el potencial de este indicador para realizar un seguimiento regular del ecosistema que permita mejorar su gestión y su conservación.

- Analizar la relación entre los cambios de estado fenológico del pasto natural y los cambios hídricos del ecosistema combinando las imágenes proporcionadas por una cámara digital terrestre, con imágenes de satélite y datos meteorológicos. Proponer indicadores de seguimiento de su fenología y estado hídrico.

I.6. Estructura de la tesis

La estructura de la tesis se presenta esquematizada en la figura I.4. Cada capítulo aborda los siguientes aspectos:

- En el presente **Capítulo 1** se plantean los antecedentes, los objetivos y la estructura de la tesis. La caracterización de las distintas variables biofísicas, prepuesta en el objetivo específico (OE) 1, se desarrolla a lo largo de todos los capítulos de la misma, ya que en cada uno de ellos una o varias variables biofísicas sirven como información de partida para obtener diferentes indicadores.

- El **Capítulo 2** desarrolla el indicador del estado hídrico del suelo a partir del vigor de las cubiertas vegetales y corresponde al OE-2.

> Gómez-Giráldez, P.J., Aguilar, C., Polo, M.J., (2014). Natural vegetation covers as indicators of the soil water content in a semiarid mountainous watershed**.** Ecological Indicators 46. 524–535. doi: 10.1016/j.ecolind.2014.06.024

- El **Capítulo 3** aborda el OE-3 y desarrolla el indicador de seguimiento de producción de pastos a partir de datos meteorológicos e información de imágenes de satélite. En este capítulo también se profundiza en el efecto del estrés hídrico en este indicador para cubiertas adehesadas, como punto de partida para futuras mejoras y revisiones del modelo.

> Gómez-Giráldez, P.J., Aguilar, C., Caño, A.B., García-Moreno, A., González-Dugo, M.P., (2019).Remote sensing estimation of net primary production as monitoring indicator of holm oak savanna management**.** Ecological Indicators, 106, 105526. Doi: https://doi.org/10.1016/j.ecolind.2019.105526

> Gómez-Giráldez, P.J., Carpintero, E., Ramos, M., Aguilar, C., González-Dugo, M.P. (2018). Effect of the water stress on gross primary production modeling of a Mediterranean oak savanna ecosystem. Proc. IAHS, 95, 1–7, 2018. Doi: https://doi.org/10.5194/piahs-95-1-2018.

- El **Capítulo 4** desarrolla el indicador que vincula la fenología del pasto y la hidrología del sistema, abordando el OE-4 .

Gómez-Giráldez, P.J., Pérez-Palazón, M.J., Polo, M.J., González-Dugo, M.P., (2020). Monitoring grass phenology and hydrological dynamics of an oak-grass savanna ecosystem using Sentinel-2 and terrestrial photography. Remote Sensing, 12, 600; doi:10.3390/rs12040600

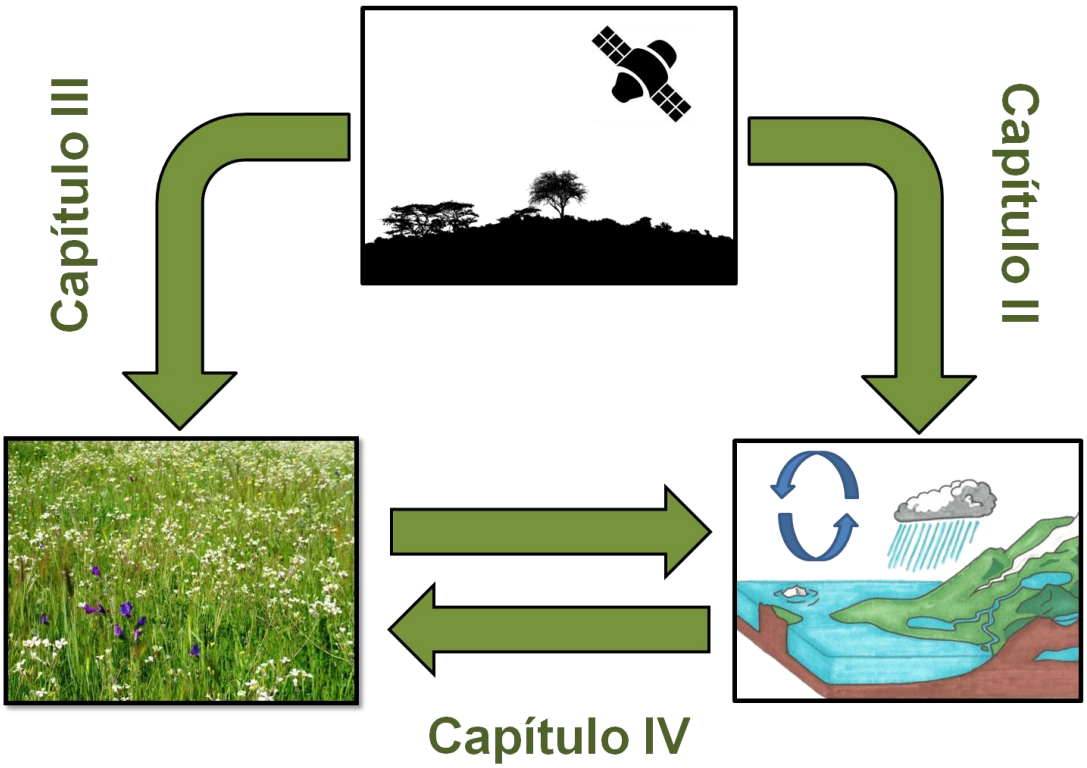

Figura I.4. Representación esquemática de los capítulos que presenta la tesis.

I.7. Referencias

Aguilar, C., Zinnert, J. C., Polo, M. J., Young, D. R., 2012. *NDVI as an indicator for changes in water availability to woody vegetation*. Ecol. Indic. 23, 290-300.https://doi.org/10.1016/j.ecolind.2012.04.008

Almeida-García, F.N., 2009. *Geografía del mundo mediterráneo*. OCW Universidad de Málaga.

Anderson, M. C., Kustas, W. P., Norman, J. M., Hain, C. R., Mecikalski, J. R., Schultz, L., … Gao, F. 2011. *Mapping daily evapotranspiration at field to continental scales using geostationary and polar orbiting satellite imagery*. Hydrol. Erth Syst. Sc., 15(1), 223–239. https://doi.org/10.5194/hess-15-223-2011

Andreu, A., Kustas, W. P., Polo, M. J., Carrara, A., & González-Dugo, M. P. 2018. *Modeling surface energy fluxes over a dehesa (oak savanna) ecosystem using a thermal based two-source energy balance model (TSEB) I*. Remote Sens, 10(4), 1–27. https://doi.org/10.3390/rs10040567

Andreu, A., Timmermans, W. J., Skokovic, D., & Gonzalez-Dugo, M. P. 2015. *Influence of Component Temperature Derivation from Dual Angle Thermal Infrared Observations on TSEB Flux Estimates Over an Irrigated Vineyard*. Acta Geophysica, 63(6), 1540–1570. https://doi.org/10.1515/acgeo-2015-0037

Aschmann, H.,1973. *Distribution and peculiarity of Mediterranean Ecosystems*. In: Mediterranean Type Ecosistems: Origin and structure. Di Castri, F. & Mooney, H. A. (eds). New York: Springer-Verlag. 405 pp.

Baker, J.C., O'Connell, K.M., Williamson, R.A.,2001. *Commercial Observation Satellites: At the Leading Edge of Global Transparency*. Santa Monica: RAND-ASPRS.

Brookes, A.J., 1975. *Photo Reconnaissance: The Operational History*. Londres: Ian Allan.

Castillo, V.M., Gómez-Plaza, A., Martínez-Mena, M., 2003. *The role of antecedent soil water content in the runoff response of semiarid catchments: a simulation approach.* J. Hydrol. 284, 114-130. https://doi.org/10.1016/S0022-1694(03)00264-6

Chaponnière, A., Boulet, G., Chehbouni, A., Aresmouk, M., 2008. *Understanding hydrological processes with scarce data in a mountain environment*. Hydrol. Process. 22, 1908–1921.https://hal.ird.fr/ird-00388861

Chuvieco, E., 1990. *Fundamentos de Teledetección Espacial*. Madrid: Ed. Rialp.

Chuvieco, E., 2002. *Teledetección Ambiental. La observación de la Tierra desde el espacio.* Barcelona: Ed. Ariel.

Cortesi, N., González-Hidalgo, J.C., Brunetti, M., & Martin-Vide, J., 2012. *Daily precipitation concentration across Europe 1971–2010*. Nat. Hazards Earth Syst. Sci., 12, 2799–2810, doi:10.5194/nhess-12-2799-2012.

Eagleson, P. S., & Segarra, R. I., 1985. *Water‐Limited Equilibrium of Savanna Vegetation Systems*. Water Resour. Res 1985 , 21(10), 1483–1493.https://doi.org/10.1029/WR021i010p01483

Ehlerinder, J.R., y Field, C.B., 1993. *Scaling Physiological Processes*. Academic Press. https://doi.org/10.1016/C2009-0-03319-4

Ellis, R. J., Taylor, C. M., Weedon, G. P., Gedney, N., Clark, D. B., Sietse, L., 2009. *Evaluating the Simulated Seasonality of Soil Moisture with Earth Observation Data*. J. Hydrometeor. 10, 1548-1560. https://www.jstor.org/stable/24912812

García-moreno, A., Fernández-Rebollo, P., Muñoz, M., & Carbonero, M., 2016. *Gestión de los pastos en la dehesa.* Instituto de Investigación y Formación Agraria y Pesquera (IFAPA). Dep. Legal CO-614-2016. https://www.juntadeandalucia.es/agriculturaypesca/ifapa/servifapa/contenidoAlf?id=1e33ce7b-9a13-4d73-8832-f367be91c551&sector=69cc80a0-9a2d-11df-accb-b374239e8181&sectorf=69cc80a0-9a2d-11df-accb-b374239e8181&l=material

Glenn, E., Huete, A., Nagler, P., Nelson, S., 2008. *Relationship Between Remotely-sensed Vegetation Indices, Canopy Attributes and Plant Physiological Processes: What Vegetation Indices Can and Cannot Tell Us About the Landscape*. Sensors, 8, 2136- 2160. https://doi.org/10.3390/s8042136

Gómez-Giráldez, P. J., Aguilar, C., Polo, M. J., 2012. *NDVI sensitivity to the hydrological regime in semiarid mountainous environments*. Proceeding. SPIE. 8531, 85311A. https://doi.org/10.1117/12.974534

Gonzalez-Dugo, M. P., Neale, C. M. U., Mateos, L., Kustas, W. P., Prueger, J. H., Anderson, M. C., Li, F. 2009. *A comparison of operational remote sensing-based models for estimating crop evapotranspiration*. Agric. For. Meteorol, 149(11), 1843–1853. https://doi.org/10.1016/j.agrformet.2009.06.012

González-Dugo, M. P., y Mateos, L. 2008. *Spectral vegetation indices for benchmarking water productivity of irrigated cotton and sugarbeet crops*. Agric Water Manag, 95(1), 48–58. https://doi.org/10.1016/j.agwat.2007.09.001

Hill, M.J., Donald, G.E., Hyder, M.W., Smith, R.C.G., 2004. *Estimation of pasture growth rate in the south west of Western Australia from AVHRR NDVI and climate data*. Remote Sens. Environ. 93, 528–545. https://doi.org/10.1016/j.rse.2004.08.006

Huete, A., Ponce-Campos, G., Zhang, Y., Restrepo-Coupe, N., Ma, X., Susan-Moran, M., 2015. *Monitoring Photosynthesis from Space*. In: Land Resources Monitoring, Modeling, and Mapping with Remote Sensing. Ed.Prasad S. Thenkabail . 3-22.

Huete, A.R.. 1988. *A soil-adjusted vegetation index*. Remote Sens. Environ., 25, 295–309. https://doi.org/10.1016/0034-4257(88)90106-X

Jin, Z., Zhuang, Q., He J.S., Luo, T. & Shi, Y., 2013. *Phenology shift from 1989 to 2008 on the Tibetan Plateau: an analysis with a process-based soil physical model and remote sensing data*. Clim. Change, vol. 119(2), pages 435-449. DOI: 10.1007/s10584-013-0722-7

Jódar, J., Carpintero, E., Martos-Rosillo, S., Ruiz-Constán, A., Marín-Lechado, C., Cabrera-Arrabal, J. A., González-Dugo, M. P. 2018. *Combination of lumped hydrological and remote-sensing models to evaluate water resources in a semi-arid high altitude ungauged watershed of Sierra Nevada (Southern Spain)*. Sci. Total Environ., 625, 285–300. https://doi.org/10.1016/j.scitotenv.2017.12.300

Klosterhalfen, A., Graf, A., Brüggemann, N., Drüe, C., Esser, O., González-Dugo, M. P., Vereecken, H. 2019. *Source partitioning of H2O and CO2 fluxes based on high-frequency eddy covariance data: A comparison between study sites*. Biogeosciences, 16(6), 1111–1132. https://doi.org/10.5194/bg-16-1111-2019

Kovats, R.S., Valentini, R., Bouwer, L.M., Georgopoulou, E., Jacob, D., Martin, E., Rounsevell, M. and Soussana, J.F., 2014. *Climate Change 2014: Impacts, Adaptation, and Vulnerability. Part B: Regional Aspects.* Contribution of Working Group II to the Fifth Assessment Report of the Intergovernmental Panel on Climate Change [Barros, V.R., C.B. Field, D.J. Dokken, M.D. Mastrandrea, K.J. Mach, T.E. Bilir, M. Chatterjee, K.L. Ebi, Y.O. Estrada, R.C. Genova, B. Girma, E.S. Kissel, A.N. Levy, S. MacCracken, P.R. Mastrandrea, y L.L.White (eds.)]. Cambridge University Press, Cambridge, UK and New York, NY, USA, 2014, pp. 1267-1326.

Maneta, M., Schnabel, S., Jetten, V., 2008. *Continuous spatially distributed simulation of surface and subsurface hydrological processes in a small semiarid catchment* Hydrol. Process. 22, 2196–2214. https://doi.org/10.1002/hyp.6817

Martín-Vide, J. y Olcina, J., 2001. *Climas y tiempos de España*. Madrid: Alianza Editorial.

Molina, C., Vidal-Abarca, M.R., Suárez, M.L., 1994. *Floods in arid south-east Spanish areas: a historical and environmental review.* In: Coping with Floods. G. Rossi (ed.): 271-278.

Nazir, R., Wani, A., Kashtwari, M., Beigh, Z. 2018. *Phenological shifts due to climate change and the associated conservation threats*. Clim. Change, 4 (13), 80-86.

Norrant, C. & Douguédroit, A., 2006. *Monthly and daily precipitation trends in the Mediterranean (1950–2000)*. Theor. Appl. Climatol, 83, 89–106, doi:10.1007/s00704-005-0163-y.

Padilla, F.L.M., González-Dugo, M.P., Gavilán, P., Domínguez, J. 2011. *Integration of vegetation indices into a water balance model to estimate evapotranspiration of wheat and corn*. Hydrol. Earth Syst. Sci., 15, 1213–1225. https://doi.org/10.5194/hess-15-1213-2011

Pastor-Guzman, J., Dash, J., Atkinson, P. 2018. Remote sensing of mangrove forest phenology and its environmental drivers. Remote Sens. Environ. 205, 71-84. https://doi.org/10.1016/j.rse.2017.11.009

Peña-Barragán, J.M., Ngugi, M.K., Plant, R.E. & Six, J. 2011 *Object-based crop identification using multiple vegetation indices, textural features and crop phenology*. Remote Sens. Environ., 115, 1301-1316. https://doi.org/10.1016/j.rse.2011.01.009

Poenaru, V., Badea, A., Dana Negula, I., & Moise, C. 2017. *Monitoring Vegetation Phenology in the Braila Plain Using Sentinel 2 Data*. Scientific Papers. Series E. Land Reclamation, Earth Observation & Surveying, Environmental Engineering, VI, 175–180. Retrieved from https://scihub.copernicus.eu/

Proyecto de investigación BioBio (*Indicadores de Biodiversidad de sistemas agrarios ecológicos y de bajos insumos*, EU FP7, KBBE-227161, 2009–2012).

Rivas-Martínez, 1987. *Memoria del Mapa de Series de Vegetación de España 1:400.000*. ICONA, Madrid

Robles, S., Toro, M., Nuño, C., Avilés, J., Alba-Tercedor, J., Álvarez, M., Bonada, N., Casas, J., Jáimez-Cuéllar, P., Mellado, A., Munné, A., Pardo, I., Prat, N., Suárez, M.L., Vidal-Abarca, M.R., Vivas, S., Moyá, G., Ramon, G., 2002. *Descripción de las cuencas mediterráneas seleccionadas en el proyecto GUADALMED*. Limnetica 21(3-4): 35-61. Asociación Española de Limnología, Madrid. Spain. ISSN: 0213-8409

Skakun, S., Vermote, E., Franch, B., Roger, J., Kussul, N., Ju, J., Masek, J., 2019. *Winter wheat yield assessment from Landsat 8 and Sentinel-2 data: Incorporating surface reflectance, through phenological fitting, into regression yield models*. Remote Sens. 11(15), 1768. https://doi.org/10.3390/rs11151768

Solomon, S., Quin, D., Manning, M., Chen, Z., Marquis, M., Averyt, K., Tignort, M. & Miller, H., 2017. *Climate Change: The Physical Science Basis*. Contribution of Working Group I to the Fourth Assessment Report of the Intergovernmental Panel on Climate Change, 2017, United Kingdom and New York, USA.

Strahler, A.N. y Strahler, A.H.,1989. *Geografía física*. Barcelona: Ed. Omega.

Sundseth, K. 2010. *Natura 2000 en la región mediterránea*. Comisión Europea Dirección General de Medio Ambiente. http://ec.europa.eu/environment/nature

Xue, J., Su, B., 2017. *Significant remote sensing vegetation indices: A review of developments and applications*. J. Sens., 17. https://doi.org/10.1155/2017/1353691

Yuan, W., Chen, Y., Xia, J., Dong, W., Magliulo, V., Moors, E., Olesen, J.E., Zhang, H., 2015. *Estimating crop yield using a satellite-based light use efficiency model*. Ecol. Indic. 60, 702–709. https://doi.org/10.1016/j.ecolind.2015.08.013

Zhou, Y., Xiao, X., Wagle, P., Bajgain, R., Mahan, H., Basara, J.B., Dong, J., Qin, Y., Zhang, G., Luo, Y., Gowda, P.H., Neel, J.P.S., Starks, P.J., Steiner, J.L., 2017. *Examining the short-term impacts of diverse management practices on plant phenology and carbon fluxes of Old World bluestems pasture*. Agric. For. Meteorol. 237–238, 60–70. https://doi.org/10.1016/j.agrformet.2017.01.018

CAPÍTULO II

Natural vegetation covers as indicators of the soil water content in a semiarid mountainous watershed

Ecological Indicators 46 (2014) 524–535

Contents lists available at ScienceDirect

Ecological Indicators

journal homepage: www.elsevier.com/locate/ecolind

Natural vegetation covers as indicators of the soil water content in a semiarid mountainous watershed

Pedro J. Gómez-Giráldez [a,*], Cristina Aguilar [b], María José Polo [c]

[a] Agricultural and fishing research and training Institute, ES-14071 Córdoba, Spain
[b] Fluvial Dynamics and Hydrology, IIISTA University of Granada, CEAMA, Avda del Mediterráneo s/n, Granada, 18006, Spain
[c] Fluvial Dynamics and Hydrology Research Group, Interuniversity Institute for Research on the Earth System in Andalusia, University of Cordoba, Campus Rabanales, Edificio Leonardo Da Vinci, Área de Ingeniería Hidráulica, 14017 Córdoba, Spain

ARTICLE INFO

Article history:
Received 2 February 2014
Received in revised form 10 June 2014
Accepted 17 June 2014

Keywords:
NDVI
Landsat-TM
Hydrological modeling
Water stress
Soil moisture
WiMMed

ABSTRACT

This paper investigates the use of the vegetative state of natural covers as an indicator of soil moisture conditions at the end of the dry season in order to evaluate the cumulative effect of the hydrological regime. To achieve this, the three major vegetation covers in a mountainous semiarid environment in southern Spain were selected. Temporal and spatial trends of NDVI from Landsat-TM images were computed and related to the different hydrological patterns of variables in the study site, which were obtained with the hydrological WiMMed model. The heterogeneity in the hydrological behavior during the study period (914.5 mm of annual rainfall in the wettest year (2009–2010) and 284.4 mm in the driest year (2004–2005)) was reflected in the annual differences in NDVI values with steady mean NDVI values in coniferous vegetation (0.5–0.6) and more variable values in scrub cover. Both Correlation Analysis and Principal Component Analysis showed correlations among the different states of the vegetation cover, the variables involved in the soil water balance and those related to the snow dynamics of the antecedent year. Exponential fits were obtained between the mean annual soil water content and NDVI values with Pearson r^2 coefficients of over 0.7 in scrub cover. In certain years, the best fits were also found in scrub cover with r^2 values of up to 0.9. These results demonstrate the relationship between soil water content, the vigor of the natural vegetation and the hydrological characteristics of the antecedent year. The expressions obtained may serve to adjust the soil water content at the beginning of a hydrological year and to use the scrub cover as an indicator of the soil water balance in the area for a given year.

1. Introduction

Distributed hydrological models at the watershed scale require the calibration of the parameters involved in the computation of hydrological processes (Refsgaard, 1997). The number of parameters depends on the complexity of the model in terms of the spatial and temporal discretization applied by the model to solve the hydrological cycle. The calibration process is always carried out with water flow data registered at certain control stations in the watershed (Chaponnière et al., 2008; Moussa et al., 2007). However, other intermediate variables calculated by the models (e.g. infiltration, soil moisture, runoff, etc.) could be used in the calibration process, especially under situations with scarce water flow data. This is crucial in semiarid areas where the absence of hydrological response at the outlet of the watershed, for most of the time, makes it impossible to evaluate the internal status of the watershed (Maneta et al., 2008). However, a combination of both the technical difficulties in measuring intermediate variables at the watershed scale on a regular basis and financial issues mean that hydrographs are more commonly used instead.

Soil moisture constitutes the main state variable in the soil vadose zone, since it determines the partition of rainfall into infiltration and runoff in a storm event, and the loss of moisture between storm events. In Mediterranean areas, runoff events are often caused by high-intensity storms of a short duration (Moussa et al., 2007) and reduced to a limited number of runoff events per year. They are largely determined by antecedent soil moisture conditions (Castillo et al., 2003) and thus, their calibration in continuous hydrological modeling constitutes a major problem in semiarid areas.

* Correspondence to: IFAPA—Área de Producción Agraria, Consejería de Agricultura, Pesca y Desarrollo rural, Centro Alameda del Obispo Apdo. 3092, 14080 Córdoba, Spain. Tel.: +34 669205615.
E-mail address: pjgomezgiraldez@gmail.com (P.J. Gómez-Giráldez).

http://dx.doi.org/10.1016/j.ecolind.2014.06.024
1470-160X/

CAPÍTULO III

III.1 Remote sensing estimation of net primary production as monitoring indicator of holm oak savanna management

III.2 Effect of the water stress on gross primary production modeling of a Mediterranean oak savanna ecosystem

Ecological Indicators 106 (2019) 105526

Contents lists available at ScienceDirect

Ecological Indicators

journal homepage: www.elsevier.com/locate/ecolind

Remote sensing estimation of net primary production as monitoring indicator of holm oak savanna management

Pedro J. Gómez-Giráldez[a,*], Cristina Aguilar[b], Antonia Belén Caño[a], Alma García-Moreno[a], María P. González-Dugo[a]

[a] IFAPA, Institute of Agricultural and Fisheries Research and Training of Andalusia, Avd. Menéndez Pidal s/n, 14071 Cordoba, Spain
[b] Fluvial Dynamics and Hydrology Research Group, Interuniversity Institute for Research on the Earth System in Andalusia, University of Cordoba, Campus Rabanales, Edificio Leonardo Da Vinci, 14017 Córdoba, Spain

ARTICLE INFO

Keywords:
LUE-model
MODIS
SENTINEL-2
Dehesa

ABSTRACT

The management of large areas such as the *dehesa* (a multifunctional agrosilvopastoral system), with approximately 3 million ha in the Iberian Peninsula, requires effective tools to help decision-making on different scales. This work focuses on the monitoring of pasture production using remote sensors. An adaptation of a Light Use Efficiency (LUE) model has been applied using meteorological data and satellite images on two scales: Regional scale – the *dehesa* area of Andalusia (Southern Spain) with data of the MODerate resolution Imaging Spectroradiometer (MODIS, MOD09Q1 product) during the hydrological years 2013/2104 and 2014/2015; on a field scale – after pasture improvements, using the earth observation satellites SENTINEL-2 during the hydrological years 2015–2016 and 2016–2017.

The adaptation of the model proposed in this work pays special attention to: the spatial and temporal interpolation of meteorological variables; the presence of a tree layer as part of the ecosystem that influences spectral data and needs to be taken into account and subtracted accordingly; the estimation of the fraction of photosynthetically active radiation absorbed by the pasture (*fPAR*); and the empirical estimation of the light use efficiency for natural grasslands, using biomass field measurements.

The results obtained presented an error of around 13%, considered adequate for the applications addressed in this study, suggesting that this approach can be useful as an indicator for monitoring the net primary production in this ecosystem.

1. Introduction

The Mediterranean oak savanna (known as *dehesa* in Spain and *montado* in Portugal) is one of the most distinctive and representative agrosilvopastoral systems in Europe, covering around 3.1 million hectares in Spain and Portugal (Moreno and Pulido, 2008). It is an open forest, populated primarily by holm oaks (*Quercus ilex*), but cork oak (*Quercus suber*), Portuguese oak (*Quercus faginea*) or wild olives (*Olea europaea* var *sylvestris*) often appear. The sparse structure of the system allows the proliferation of pastures for livestock and wildlife, fostering a multiple use of the land, which also provides important ecosystem services such as soil protection or the conservation of key habitats for biodiversity, as well as important cultural and historical values.

The conservation of the system requires a continuous human intervention to keep up an adequate structure, and a balance of key canopy components. In the last decades, several threats have endangered this conservation. These are: mainly lack of tree regeneration, the loss of fertile soil by erosion, a strong incidence of root rot caused by soilborne pathogen *Phytophthora cinnamomi* (Pulido and Picardo, 2010) and an increase in aridity and rainfall torrentiality that may be exacerbated in the future by climate change conditions (Collins et al., 2013; Nunes et al., 2017). In addition, social and economic aspects, such as the low profitability and the aging of the workforce associated with these systems, suggest the need for a renewal of management practices and conservation policies aiming at improving the sustainability and resilience of the system (Gómez-Giráldez et al., 2016).

One of the main products of these areas, the annual pastures used for livestock feed, seems to be decreasing in recent years according to the biomass reduction trend observed in the southwest of the Iberian Peninsula (Giner et al., 2012). This reinforces the need for a close monitoring of this ecosystem, and the development of effective indicators, timely and accurate for assessing the vegetation status and

* Corresponding author.
E-mail address: pjgomezgiraldez@gmail.com (P.J. Gómez-Giráldez).

https://doi.org/10.1016/j.ecolind.2019.105526
Received 18 June 2018; Received in revised form 5 March 2019; Accepted 25 June 2019

Proc. IAHS, 95, 1–7, 2018
https://doi.org/10.5194/piahs-95-1-2018

Effect of the water stress on gross primary production modeling of a Mediterranean oak savanna ecosystem

Pedro J. Gómez-Giráldez[1], Elisabet Carpintero[2], Mario Ramos[2], Cristina Aguilar[1], and María P. González-Dugo[2]

[1]Fluvial dynamics and hydrology research group, Andalusian Institute of Earth System Research, University of Córdoba, 14071 Córdoba, Spain
[2]IFAPA Consejería de Agricultura Pesca y Desarrollo Rural, Apdo 3048, 14071 Córdoba, Spain

Correspondence: Pedro Jesús Gómez-Giráldez (pjgomezgiraldez@gmail.com)

Received: 17 April 2018 – Revised: 16 July 2018 – Accepted: 19 July 2018 – Published:

Abstract. *Dehesa* ecosystem consists of widely-spaced oak trees combined with crops, pasture and Mediterranean shrubs. It is located in the southwest of the Iberian Peninsula, where water scarcity is recurrent, severely affecting the multiple productions and services of the ecosystem. Upscaling in situ Gross Primary Production (GPP) estimates in these areas is challenging for regional and global studies, given the significant spatial variability of plant functional types and the vegetation stresses usually present. The estimation of GPP is often addressed using light use efficiency models (LUE-models). Under soil water deficit conditions, biomass production is reduced below its potential rate. This work investigates the effect of different parameterizations to account for water stress on GPP estimates and their agreement with observations. Ground measurements of GPP are obtained using an Eddy Covariance (EC) system installed over an experimental site located in Córdoba, Spain. GPP is estimated with a LUE-model in the footprint of the EC tower using several approaches: a fixed value taken from previous literature; a fixed value modified by daily weather conditions; and both formulations modified by an additional coefficient to explicitly consider the vegetation water stress. The preliminary results obtained during two hydrological years (2015/2016 and 2016/2017) are compared, focusing on specific wet and dry periods.

1 Introduction

Dehesa (known as *montado* in Portugal) ecosystem combines forest, agricultural and extensive livestock productions, presenting important ecosystem services and cultural values. It is composed of sparse trees (mainly holm oak) and an undergrowth of shrub, pasture or herbaceous crop, constituting a characteristic landscape of the southwest of the Iberian Peninsula (Parsons, 1962).

This landscape is characterized by the low fertility of the soils, not suitable for regular farming, and a Mediterranean climate with a high vulnerability to global warming, with increasingly extreme droughts and torrential rainfalls (Kovats et al., 2014).

The assimilation of CO_2 due to the vegetation is represented by the gross primary production (GPP). This production is often estimated from remote sensing based on the works of Monteith (1972) that use biophysical variables and subsequently validated with eddy covariance (EC) systems (e.g. Migliavacca et al., 2009; Wagle et al., 2014; Zhang et al., 2015). These models, known as light use efficiency (LUE) models, relate the incident solar radiation with the photosynthetic activity of the plant, or canopy, through a LUE parameter, which is the amount of biomass produced per unit of radiation absorbed. Under soil water deficit conditions, biomass production is reduced below its potential rate, but this effect is sometimes addressed only indirectly by these models.

The objective of this work is to test different approaches to consider water stress on GPP estimates over a *dehesa* ecosystem using a LUE-model. GPP has been estimated with a LUE-model using field data, Sentinel-2 images, meteorological information and several LUE approaches: a fixed value;

Published by Copernicus Publications on behalf of the International Association of Hydrological Sciences.

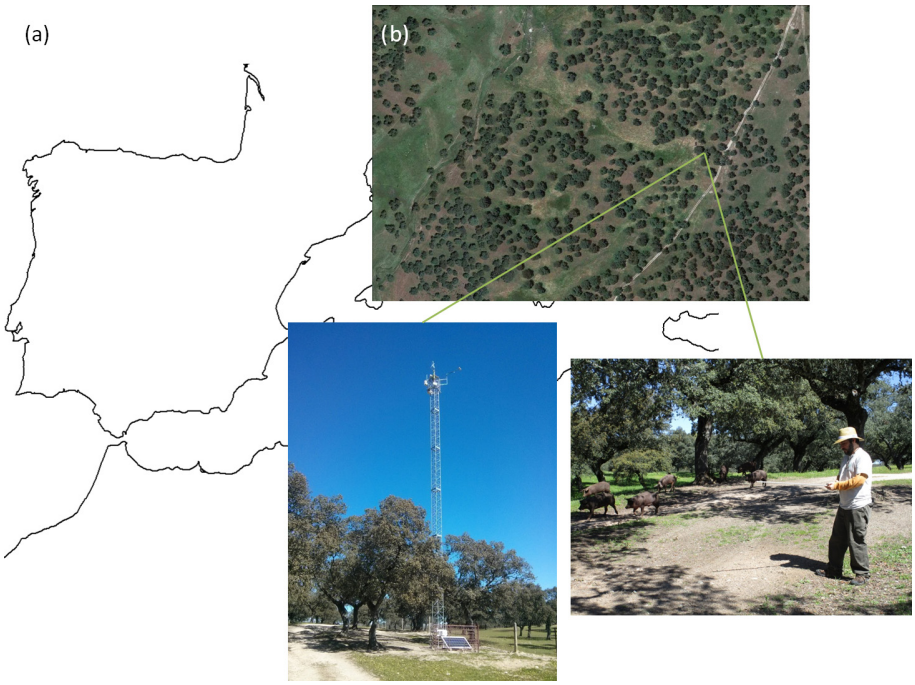

Figure 1. Study site **(a)**, Aerial photography of the area **(b)**, EC tower **(c)** and field measurements example **(d)**.

a fixed value modified by daily weather conditions; and both formulations with an additional coefficient to explicitly consider the vegetation water stress. The results were compared to those obtained from an EC system from July 2015 to September 2017, analyzing the behavior of the selected approaches at different temporal scales.

2 Material and methods

2.1 Study site and eddy covariance data

The study site is a farm located in Cardeña (Córdoba, Spain) (Fig. 1a), part of an environmental protected area. It presents an average rainfall of 720 (±150) mm per year, cold winters, long and dry summers and periodic severe droughts.

The EC system is installed in a gently sloped area with uniform fetch (length in the prevailing wind direction) and homogeneous vegetation (holm oak and pasture) (Fig. 1b and c). The equipment is located at 18 m above ground level in order to minimize the effect of roughness (trees present 7-8 meters of height). A limited number of available measurements caused by a loss of data of the EC tower during one month occurred in the first trimester of 2016. GPP was estimated using Eq. (1):

$$\mathrm{GPP} = \mathrm{NEE} - R_{\mathrm{eco}} \tag{1}$$

where NEE is the net ecosystem exchange given by the EC and R_{eco} is the respiration of the heterotrophic part of the ecosystem which was calculated by a day-time based flux-partitioning algorithm (Lasslop et al., 2010).

2.2 Application of a LUE-model

The GPP was estimated using an adaptation of Monteith (1972) model (Eq. 2):

$$\mathrm{GPP} = \mathrm{fPAR}\ \mathrm{PAR}\varepsilon \tag{2}$$

where GPP ($\mathrm{g\,m^{-2}}$) is the gross primary production, fPAR (dimensionless) is the fraction of photosynthetically active radiation absorbed by the vegetation, PAR ($\mathrm{MJ\,m^{-2}}$) is the photosynthetically active radiation and ε ($\mathrm{g\,MJ^{-1}}$) is the light use efficiency.

2.2.1 Estimation of fPAR

Sentinel-2 images and field measurements have been combined to estimate fPAR. A set of 55 Sentinel-2 cloud-free images were selected (Fig. 2a) and the NDVI was calculated using bands 4 (red) and 8 (NIR) (Fig. 2b) for the study period. The resulting images were linearly interpolated pixel by pixel to obtain a daily NDVI image with 10 m of spatial resolution.

For the transformation NDVI to fPAR, holm oaks and the pasture were addressed separately. For the holm oak, fPAR was monthly monitored by measuring 15 selected trees from the footprint area of the EC during the study period with a LP-80 ceptometer (Fig. 1d) and computing an average from these values that was used as constant value per month. For the pasture, it was used a linear relationship of NDVI-fPAR determined from satellite data in a previous study over the same area (Gómez-Giráldez et al., 2018). The separation

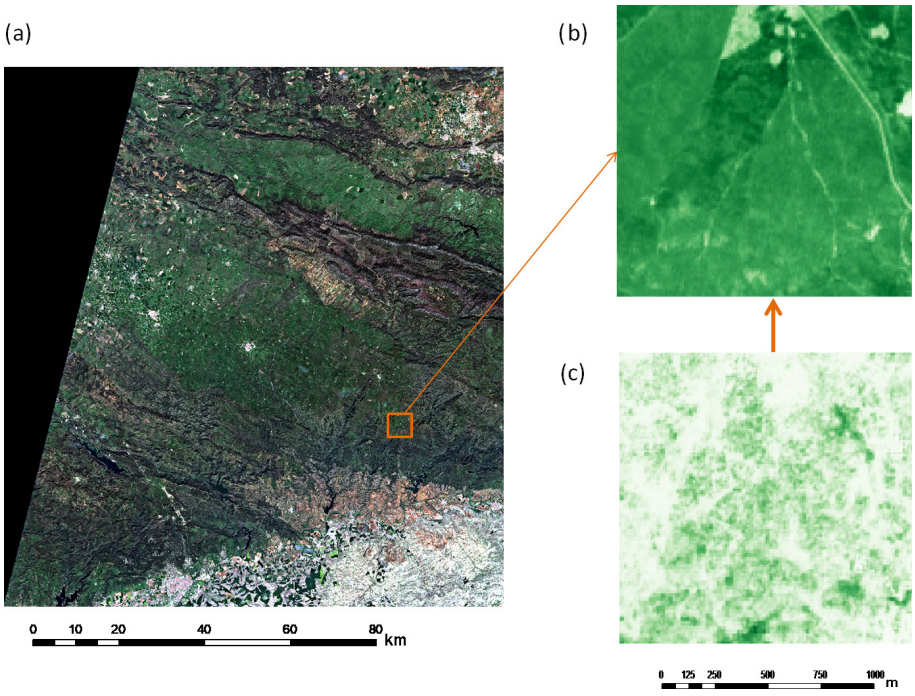

Figure 2. RGB Sentinel-2a image (7 April 2016) **(a)**, NDVI (7 April 2016) **(b)** and fcover images (28 July 2017) **(c)**.

between tree and pasture at pixel level was done assuming that the spectral response of both canopies is additive (e.g. Lu et al., 2003; Blanco et al., 2016). To differentiate the percentage of trees and pasture in each pixel, the coverage fraction image (fcover) was obtained using SNAP toolbox by ESA (http://step.esa.int/main/toolboxes/snap/, last access: 25 July 2018). The Sentinel-2 image of 28 July 2017 was used as reference (Fig. 2c). On this date, the pasture is totally dry and the fcover corresponded only to the tree canopy and can be considered constant.

With these premises, Eq. (3) was obtained:

$$\mathrm{fPAR} = \mathrm{fPAR}_{\mathrm{oak}}\mathrm{fcover} + \mathrm{fPAR}_{\mathrm{pasture}}(1 - \mathrm{fcover}). \quad (3)$$

Finally, to obtain a daily value representative of EC footprint area, a daily footprint function was calculated and used to weigh image pixels. The final data is the sum of the product of fPAR and footprint weights.

2.2.2 Estimation of PAR

The PAR estimation is computed using daily values of solar radiation measured with a 4-component net radiometer NR-1 and a reducing factor of 0.48 according to Szeicz (1974), obtained from measurements in a set of points distributed throughout the globe.

2.2.3 Estimation of ε

A maximum value ($\varepsilon_{\max}$) of 0.77 was selected, based on the results obtained by Running et al. (2000) for wooded grassland. Four methods were analysed:

1. *Max*: the use of $\varepsilon_{\max}$ to test the need to attenuate it.
2. *Meteo*: it uses the attenuation proposed by Running et al. (2000) considering the climatic variables that reduce the efficiency of the plant: minimum daily temperature ($T_{\min}$) and the vapour pressure deficit (VPD). A scalar minimum temperature and the scalar VPD, which are simple linear ramp functions between 0 and 1 derived from the daily values of $T_{\min}$ and VPD. These linear function are obtained using threshold values, where the minimum and maximum value for $T_{\min}$ correspond to 0 and 1 vales of scalar $T_{\min}$ (increasing function) respectively; and minimum and maximum value for VPD correspond to 1 and 0 vales of scalar VPD (decreasing function respectively). The threshold values used were: -8 and 11.39 °C for $T_{\min}$, and 0.65 and 3.1 kPa for VPD.
3. W: the use of an attenuation factor due to the water stress of the ecosystem computed by Eq. (4):

$$W = \frac{\mathrm{ET}}{\mathrm{ET_r}} \quad (4)$$

where W (dimensionless) is the water stress coefficient multiplying $\varepsilon_{\max}$ value; ET (mm day^{-1}) is the

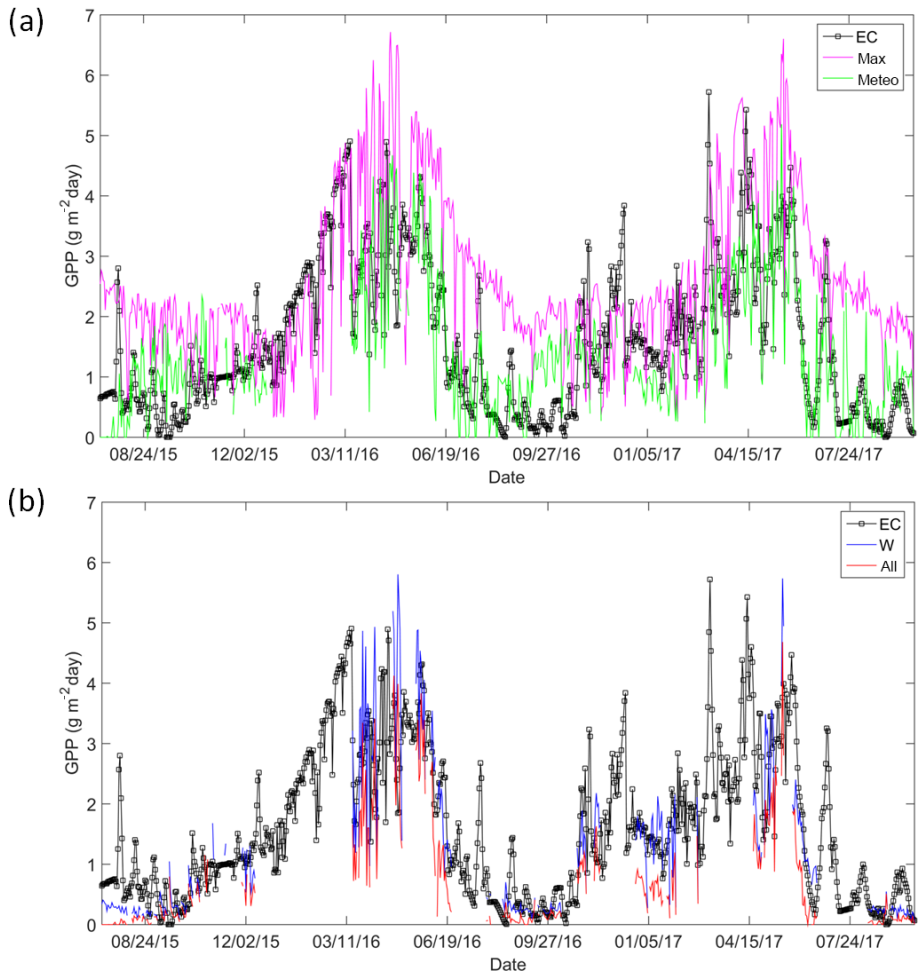

Figure 3. Temporal profile of the GPP fluxes: **(a)** EC, *max* and *meteo* **(b)** EC, *W* and *all*.

daily evapotranspiration of the system by the method of Bowen (1926); and ET_r (mm day^{-1}) is the reference evapotranspiration estimated by the Hargreaves formula (Hargreaves and Samani, 1985).

4. *All*: this approach consider the application of the two previous attenuations, reducing the ε_{max} by multiplying both, *W* and the scalar VPD and T_{min}.

All the meteorological data required for the calculations were obtained from half-hour measurements of the EC system.

2.3 Study of the methods

In order to study the 4 methods at different temporal scales, the correlation coefficient (R^2) of the linear regressions, the root mean squared error (RMSE) and the Mean Absolute Percentage error (MAPE) of the four methods were calculated at different temporal scales: (i) daily data was analysed for the entire study period; (ii) average values were computed for each of the two hydrological years (1 October to 30 September) 2015/2016 and 2016/2017; (iii) data was averaged in terms of wet (1 October to 15 May) and dry periods (15 May to 30 September).

Finally, the accumulated values for each hydrological year and period were obtained and compared to the measurements of the EC.

3 Results and discussion

The values obtained for fPAR and *W* for the area vary between 0.2 and 0.7, and 0.03 and 1.10, respectively with average values for the study period of 0.44 and 0.38. Both variables presented a high variability, representative of the Mediterranean climate and vegetation. The average values for ε along the study period were: 0.3 g MJ^{-1} for *meteo* method, 0.29 g MJ^{-1} for *W* method and 0.14 for *all* method.

Figure 3 shows the temporal profile of GPP at daily scale obtained by the EC and estimated with the four methods considered. The seasonal variation of GPP along the study period can be appreciated, with clear differences between wet and dry periods.

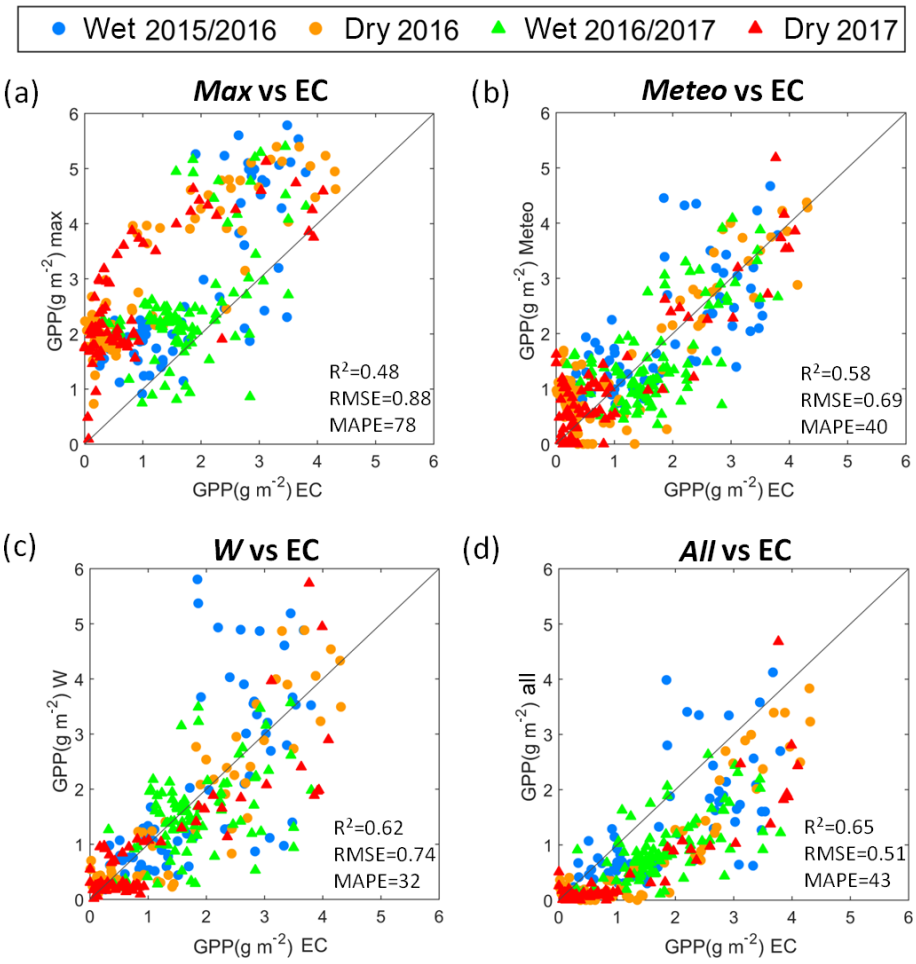

Figure 4. Comparison of GPP measured by the EC vs. max **(a)**, EC vs. meteo **(b)**, EC vs. *W* **(c)** and EC vs. all **(d)**. Blue: wet period; orange: dry period; circle: 2015/2016; triangle: 2016/2017; black line: 1 : 1 line.

The method *max* (Fig. 4a) presented the weakest correlation (0.48) as expected, the highest error (RMSE = 0.88 g m^{-2}; MAPE = 78 %) and a general overestimation. The *meteo* method (Fig. 4b) improved the results which were similar to those of the *W* method (Fig. 4c) with no significant biases. Finally, despite the method *all* (Fig. 4d) underestimated the GPP (MAPE = 43 %), it presented the best correlation (0.65) and lower RMSE (0.51 g m^{-2}). The correlation values obtained using *W* were lower than those obtained previously by Gilabert et al. (2015), but this difference could be explained by the significant higher spatial resolution of this analysis, 10 m, compared to the aggregation at 1 km of their study.

It can be appreciated that there are very low values in summer when the photosynthetic activity is lower. The pasture is dry and not contributing, and the stomata of the trees are often closed. The methods *W* and *all* performed poorly in this range of very low GPP values. The other cases (*max* and *meteo*) did not present this effect because they overestimated GPP.

The results obtained for both hydrological years (Table 1) were of similar order of magnitude.

The results obtained during the wet periods (Table 1) presented the poorest correlations. The 2016/2017 wet period presented an analogous behaviour, in terms of correlations and errors, compared to that obtained with the whole hydrological year but with lower correlation values. However, the 2015/2016 wet period showed a similar correlation value (around 0.4) in all methods possibly due to the gap in EC.

The results for the dry periods showed the highest correlation (over 0.8 and 0.7 in 2016 and 2017 respectively) but with higher dispersion (higher MAPE than wet period) and the use of the water stress factor improved the results. This difference between the periods confirms the findings of previous studies (e.g. Heinsch et al., 2006).

Finally, Table 2 presents the accumulated GPP values and the differences in percentage with respect to the EC data.

Comparing the accumulated GPP the *max* method strongly overestimated the GPP, in both dry periods (around 150 %) and wet periods (around 50 %). *All* underestimated about a

Table 1. R^2, RMSE ($g\,m^{-2}$) and MAPE (%) obtained by comparison with EC measurements for 2015/2016 and 2016/2017 in the four methods, and over wet and dry periods.

Hydorological year					
2015/2016	R^2	RMSE (MAPE)	2016/2017	R^2	RMSE (MAPE)
max	0.57	0.87 (76)	*max*	0.40	0.86 (82)
meteo	0.58	0.74 (36)	*meteo*	0.59	0.64 (45)
W	0.64	0.84 (34)	*W*	0.62	0.60 (30)
all	0.65	0.59 (42)	*all*	0.68	0.40 (44)
Wet period					
2015/2016	R^2	RMSE (MAPE)	2016/2017	R^2	RMSE (MAPE)
max	0.52	1.15 (43)	*max*	0.28	0.90 (49)
meteo	0.46	0.77 (30)	*meteo*	0.40	0.70 (40)
W	0.47	1.10 (35)	*W*	0.30	0.67 (29)
all	0.44	0.75 (36)	*all*	0.44	0.43 (44)
Dry period					
2016	R^2	RMSE (MAPE)	2017	R^2	RMSE (MAPE)
max	0.77	0.6 (149)	*max*	0.65	0.75 (158)
meteo	0.80	0.41 (47)	*meteo*	0.70	0.61 (48)
W	0.84	0.52 (31)	*W*	0.73	0.53 (39)
all	0.84	0.41 (48)	*all*	0.75	0.40 (55)

Table 2. Accumulated GPP ($g\,m^{-2}\,day^{-1}$) for hydrological year and wet and dry period. The percentage represents the difference respect to EC data.

Hydrological year					
2015/2016	GPP	%	2016/2017	GPP	%
EC	273.9		EC	238.7	
max	562.2	+105.2	*max*	473.9	+98.5
meteo	282.4	+3.1	*meteo*	245.6	+2.9
W	248.4	−9.3	*W*	204.9	−14.2
all	147.0	−46.3	*all*	117.1	−50.9
Wet period					
2015/2016	GPP	%	2016/2017	GPP	%
EC	133.6		EC	160.0	
max	214.2	+60.4	*max*	232.2	+45.1
meteo	133.2	−0.3	*meteo*	142.3	-11.0
W	138.2	−3.4	*W*	137.4	+14.1
all	85.7	−35.8	*all*	82.2	−48.6
Dry period					
2016	GPP	%	2017	GPP	%
EC	101.7		EC	72.5	
max	241.3	+137.3	*max*	198.2	+173.4
meteo	118.6	+16.6	*meteo*	82.7	+14.1
W	96.7	-4.9	*W*	61.8	−14.8
all	57.0	−43.9	*all*	32.1	−55.7

45 % independently dry or wet period. *Meteo* attenuation results obtained for hydrological year and especially for wet period were the most accurate (11 % or less). *W* attenuation was the most accurate for dry periods (differences lower than 15 %), results that agree with other studies as Dong et al. (2015).

4 Conclusions

This study explored different approaches to estimate GPP considering environmental factors and present a preliminary assessment of four different methods. On a daily scale, the combined use of a water stress index and meteorological attenuation provided better GPP estimates regarding R^2 and RMSE than the other formulations, especially for the dry season. However, this method presented a bias at daily scale that for the accumulated values resulted in a significant underestimation of seasonal values.

The use of a fixed value of ε presented the poorest results, supporting the need for environmental attenuation factors, as the approaches tested here. *Meteo* and *W* provided similar estimates, even when the nature of the attenuation considered was different. Further analysis of these factors is required to propose a specific model suited to *dehesa* ecosystem.

Data availability. Data sets are available upon request by contacting the correspondence author.

Author contributions. PJG-G and MPG-D conceived and designed the experiments; PJG-G, EC and MR performed the experiments; PJG-G analysed the data and wrote the article and CA and MPG-D contributed to the interpretation of data and reviewed the article.

Competing interests. The authors declare that they have no conflict of interest.

Special issue statement. This article is part of the special issue "Earth Observation for Integrated Water and Basin Management: New possibilities and challenges for adaptation to a changing environment". It is a result of The Remote Sensing & Hydrology Symposium, Cordoba, Spain, 8–10 May 2018.

Acknowledgements. This work has been funded byLIFE+bioDehesa project (LIFE11/BIO/ES/000726) and INIA-FEDER 2014–2020 (Operational Programme Smart Growth) project RTA2014-00063-C04-02.

Edited by: Rafael Pimentel
Reviewed by: three anonymous referees

References

Blanco, L. J., Paruelo, J. M., Oesterheld, M., and Biurrun, F. N.: Spatial and temporal patterns of herbaceous primary production in semi-arid shrublands: a remote sensing approach, J . Veg. Sci., 27, 716–727, 2016.

Bowen, I. S.: The ratio of heat losses by conduction and by evaporation from any water surface, Phys. Rev., 27, 779–787, 1926.

Dong, J., Xiao, X., Wagle, P., Zhang, G., Zhou, Y., Jin, C., Torn, M. S., Meyers, T. P., Suyker, A. E., Wang, J., Yan, H., Biradar, C., and Moore, B.: Comparison of four EVI-based models for estimating gross primary production of maize and soybean croplands and tallgrass prairie under severe drought, Remote Sens. Environ. 162, 154–168, 2015.

Gilabert, M. A., Moreno, A., Maselli, F., Martínez, B., Chiesi M., Sánchez-Ruiz, S., García-Haro, F. J., Pérez-Hoyos, A., Campos-Taberner, M., Pérez-Priego, O., Serrano-Ortiz, P., and Carrara, A.: Daily GPP estimates in Mediterranean ecosystems by combining remote sensing and meteorological data, ISPRS J. Photogramm., 102, 184–197, 2015.

Gómez-Giráldez, P. J., Aguilar, C., Caño, A. B., García, A., and González-Dugo, M. P.: Remote sensing estimate of net primary production as monitoring indicator of holm oak savanna management, Ecol. Indicat. J., in review, 2018.

Hargreaves, G. H. and Samani, Z. A.: Reference crop evapotranspiration from temperature, Appl. Eng. Agr., 1, 96–99, 1985.

Heinsch, F. A., Zha, M., Running, S. W., Kimball, J. S., Nemani, R. R., Davis, K. J., and Bolstad, P. V.: Evaluation of remote sensing based terrestrial productivity from MODIS using regional tower eddy flux network observations, IEEE T. Geosci. Remote, 44, 1908–1925, 2006.

Kovats, R. S., Valentini, R., Bouwer, L. M., Georgopoulou, E., Jacob, D., Martin, E., Rounsevell, M., and Soussana, J. F.: Climate Change 2014: Impacts, Adaptation, and Vulnerability. Part B: Regional Aspects, in: Contribution of Working Group II to the Fifth Assessment Report of the Intergovernmental Panel on Climate Change, edited by: Barros, V. R., Field, C. B., Dokken, D. J., Mastrandrea, M. D., Mach, K. J., Bilir, T. E., Chatterjee, M., Ebi, K. L., Estrada, Y. O., Genova, R. C., Girma, B., Kissel, E. S., Levy, A. N., MacCracken, S., Mastrandrea, P. R., and White, L. L., Cambridge University Press, Cambridge, UK and New York, NY, USA, 1267–1326, 2014.

Lasslop, G., Reichstein, M., Papale, D., Richardson, A., Arneth, A., Barr, A., Stoy, P., and Wohlfahrt, G.: Separation of net ecosystem exchange into assimilation and respiration using a light response curve approach: critical issues and global evaluation, Global Change Biol., 16, 187–208, 2010.

Lu, H., Raupach, M., McVicar, T., and Barrett, D.: Decomposition of vegetation cover into woody and herbaceous components using AVHRR NDVI time series, Remote Sens. Environ., 86, 1–18, 2003.

Migliavacca, M., Meroni, M., Busetto, L., Colombo, R., Zenone, T., Matteucci, G., Manca, G., and Seufert, G.: Modeling Gross Primary Production of Agro-Forestry Ecosystems by Assimilation of Satellite-Derived Information in a Process-Based Model, Sensors, 9, 922–942, 2009.

Monteith, J. L.: Solar radiation and productivity in tropical ecosystems, J. Appl. Ecol., 9, 747–766, 1972.

Parsons, J. D.: The Acorn-Hog Economy of the Oak Woodlands of Southwestern Spain, Geogr. Rev., 2, 211–235, 1962.

Running, S. W., Thorton, P. E., Nemani, R., and Glassy, J. M.: Global terrestrial gross and net primary productivity from the Earth Observing System, in: Methods in Ecosystem Science, edited by: Sala, O., Jackson, R., and Mooney, H., Springer Verlag, New York, 44–57, 2000.

Szeicz, G.: Solar radiation for plant growth, J. Appl. Ecol., 11, 617–637, 1974.

Wagle, P., Xiao, X., Torn, M. S., Cook, D. R., Matamala, R., Fischer, M. L., Jin, C., Dong, J., and Biradar, C.: Sensitivity of vegetation indices and gross primary production of tallgrass prairie to severe drought, Remote Sens. Environ., 152, 1–14, 2014.

Zhang, L. X., Zhou, D. C., Fan, J. W., and Hu, Z. M.: Comparison of Four Light Use Efficiency Models for Estimating Terrestrial Gross Primary Production, Ecol. Model., 300, 30–39, 2015.

CAPÍTULO IV

Monitoring grass phenology and hydrological dynamics of an oak–grass savanna ecosystem using Sentinel-2 and terrestrial photography

remote sensing

MDI

Article

Monitoring Grass Phenology and Hydrological Dynamics of an Oak–Grass Savanna Ecosystem Using Sentinel-2 and Terrestrial Photography

Pedro J. Gómez-Giráldez [1,*], María J. Pérez-Palazón [2], María J. Polo [2] and María P. González-Dugo [1]

[1] IFAPA. Institute of Agricultural and Fisheries Research and Training of Andalusia. Avd. Menéndez Pidal s/n, 14071 Córdoba, Spain

[2] Fluvial Dynamics and Hydrology Research Group. Andalusian Institute for Earth System Research. University of Cordoba. Campus Rabanales, Edificio Leonardo Da Vinci, Área de Ingeniería Hidráulica, 14014 Córdoba, Spain

* Correspondence: pjgomezgiraldez@gmail.com

Received: 26 December 2019; Accepted: 8 February 2020; Published: 11 February 2020

Abstract: Annual grasslands are an essential component of oak savanna ecosystems as the primary source of fodder for livestock and wildlife. Drought resistance adaptation has led them to complete their life cycle before serious soil and plant water deficits develop, resulting in a close link between grass phenology and soil water dynamics. In this work, these links were explored using a combination of terrestrial photography, satellite imagery and hydrological ground measurements. We obtained key phenological parameters of the grass cycle from terrestrial camera data using the Green Chromatic Coordinate (GCCc) index. These parameters were compared with those provided by time-series of vegetation indices (VI) obtained from Sentinel-2 (S2) satellites and time-series of abiotic variables, which defined the hydrology of the system. The results showed that the phenological parameters estimated by the S2 Normalized Difference Vegetation Index (NDVI) ($r = 0.83$, $p < 0.001$) and soil moisture (SM) ($r = 0.75$, $p < 0.001$) presented the best agreement with ground-derived observations compared to those provided by other vegetation indices and abiotic variables. The study of NDVI and SM dynamics, that was extended over four growing seasons (July 2015–May 2019), showed that the seasonality of both variables was highly synchronized, with the best agreements at the beginning and at the end of the dry seasons. However, stage changes were estimated first by SM, followed by NDVI, with a delay of between 3 and 10 days. These results support the use of a multi-approach method to monitor the phenology and the influence of the soil moisture dynamic under the study conditions.

Keywords: vegetation indices; oak –grass savanna; phenology; hydrology; Sentinel-2

1. Introduction

Monitoring the phenology of Mediterranean ecosystems is key to adequately assessing the impacts of global warming on different time scales, identifying pre-critical states in the framework of early warning decision-making systems, and establishing adaptation planning and management in the medium- to long-term time horizons. The natural variability of the climatic–hydrological regime in these areas, usually with complex spatial patterns of the vegetation that is sometimes difficult to access, makes it necessary to exploit the available data from remote sensing sources.

The holm oak savanna ecosystem of the Iberian Peninsula (known as *dehesa* in Spain and *montado* in Portugal) is an ancient system emerging as the only productive and sustainable structure able to deal with the combination of low soil fertility and the high variability of the Mediterranean climate [1]. This landscape is formed by a low density of holm oak trees, an understory of grasslands and,

occasionally, shrubs and crops of cereals and legumes. The result is a mixture of natural facto and management, making it difficult to differentiate the absolute determinants of its structure [2]. However, water availability is known to be important in the conformation of this mixture of grasses and woody plants which, as stated in [3], is the only stable state of equilibrium when a marked seasonality in water availability occurs. In this state, canopy density maximizes biomass, thus minimizing water stress [4]. Annual grasslands are an essential component of this system as the primary source of fodder for livestock, and is the main economic activity in these areas, but also contains a high richness of vascular plants supporting a wide diversity of habitats [5]. The escape mechanism—i.e., the ability for the plant to complete its life cycle before serious soil and plant water deficits develop [6]—is used by these grasses to cope with the long summer dry season and the recurrent water scarcity events of the Mediterranean climate. This results in a close link between grass phenology and soil water dynamics.

Plant phenological shifts have been observed as a result of changes in the climate [7–10]. Phenological research has advanced in developing climate–phenology models derived from ground observations [11,12] and also in improving the monitoring methods constructed from satellite information [13]. In recent years, the use of remote sensing in the study of phenology has increased thanks to a greater availability of global products, which allow one to extend these studies in space and time. In particular, the use of vegetation indices (VIs) has been generalized to determine changes in vegetation on different spatial scales, ranging from centimeters to tens of kilometers. Some examples are the use of the AVHRR (Advanced Very-High-Resolution radiometer) sensor for global studies [14–16]; broad scale analysis using MERIS (Medium Resolution Imaging Spectrometer) and MODIS (Moderate-Resolution Imaging Spectroradiometer) data for maize crops and forests [17,18]; studies on a detailed scale using Landsat or ASTER (Advanced Spaceborne Thermal Emission and Reflection Radiometer) for multiple crops monitoring [19,20]; and at a very high spatial resolution with UAVs (unmanned aerial vehicles) in vineyards [21]. The Sentinel-2 (S2) sensor, part of the European Union Copernicus Program, has provided the renewed possibility of addressing canopy phenological changes on a local scale with high spatial and temporal resolutions (10–20 m or 5 days), and an improved spectral resolution providing narrow bands in the red-edge region. Despite the short time series available (from July 2015 to present), S2 has been used for the monitoring of vegetation, addressing aspects such as phenology [22], complementing other sensor datasets such as MODIS [23] or Landsat [24], and monitoring biophysical variables through the proposal of new indices making use of the red-edge bands [25]. However, its potential for improving the accuracy of estimating the phenological transition stages has not been fully explored yet.

Remote sensing studies rely on field data of phenological parameters to explain their results. However, field monitoring requires frequent and time-consuming observations, especially over areas which are difficult to access. The use of digital terrestrial cameras offers a cost-effective solution, providing real-time and reliable information to track vegetation phenology. Previous studies have used cameras for phenological monitoring [26,27], and the creation of networks of these cameras for a more global phenological follow-up is being increasingly demanded [28]. In addition, these cameras can complement the information provided by other equipment, such as weather stations or eddy covariance systems, in a wide range of applications [29–32]. The combination of these ground observations with satellite images has also been explored [33–35], and the integration of highly detailed terrestrial photography with large-scale satellite images is a promising tool that could reduce the scale gap between phenological field and remote sensing studies.

The Mediterranean climate of this area presents a high vulnerability to global warming, with an increasing occurrence of extreme droughts and torrential rainfall. This region is projected to warm more and experience greater changes in the precipitation regime over the course of the century [36–38]. An improved knowledge of how climate and hydrology influence plant phenology is key to making appropriate decisions to cope with these threats [39]. In addition, changes in values of satellite VIs have proved to be able to reflect the heterogeneity of the hydrological behavior in this region [40]. In the same line, phenological variations, assessed by using satellite data, could be useful

for evaluating the cumulative effect of the hydrological regime over large areas, in a capacity that would not be achievable with a field observation network.

In this work, images provided by a terrestrial camera were combined with meteorological information and satellite data to provide an insight into the dynamics of phenological processes and their links with the hydrological behavior of the grassland of an oak–grass savanna ecosystem. On this basis, the objectives of the present study were: 1) to explore the potential of the S2 satellites to monitor phenological changes over grasslands using a variety of vegetation indices derived from different band combinations, both broadband and narrowband indices, taking advantage in the latter case of the new possibilities offered by the red-edge bands of these satellites, 2) identify the links between hydrology and vegetation phenology derived from terrestrial photography, evaluating the response of grass vegetation and its life cycle to changes in the main abiotic variables controlling this system, and 3) study the relationship between satellite VIs and the hydrological state of the system regarding their ability to monitor grassland phenology.

2. Material and Methods

2.1. Study Site and Datasets

The study was conducted in a *dehesa* farm, called "Santa Clotilde" (Figure 1a), located in Southern Spain (Córdoba, 38º 12′ 37″ N, 4º 17′ 24″ W, 734 m.a.s.l.) [41]. It is part of an environmentally protected area (*Sierra de Cardeña y Montoro Natural Park*) with a landscape composed of sparse holm oak trees and natural grasses. The semiarid climate in this region is characterized by cold winters and long dry summers, with periodic severe droughts. Beef cattle and pigs are raised extensively on grasslands and acorns.

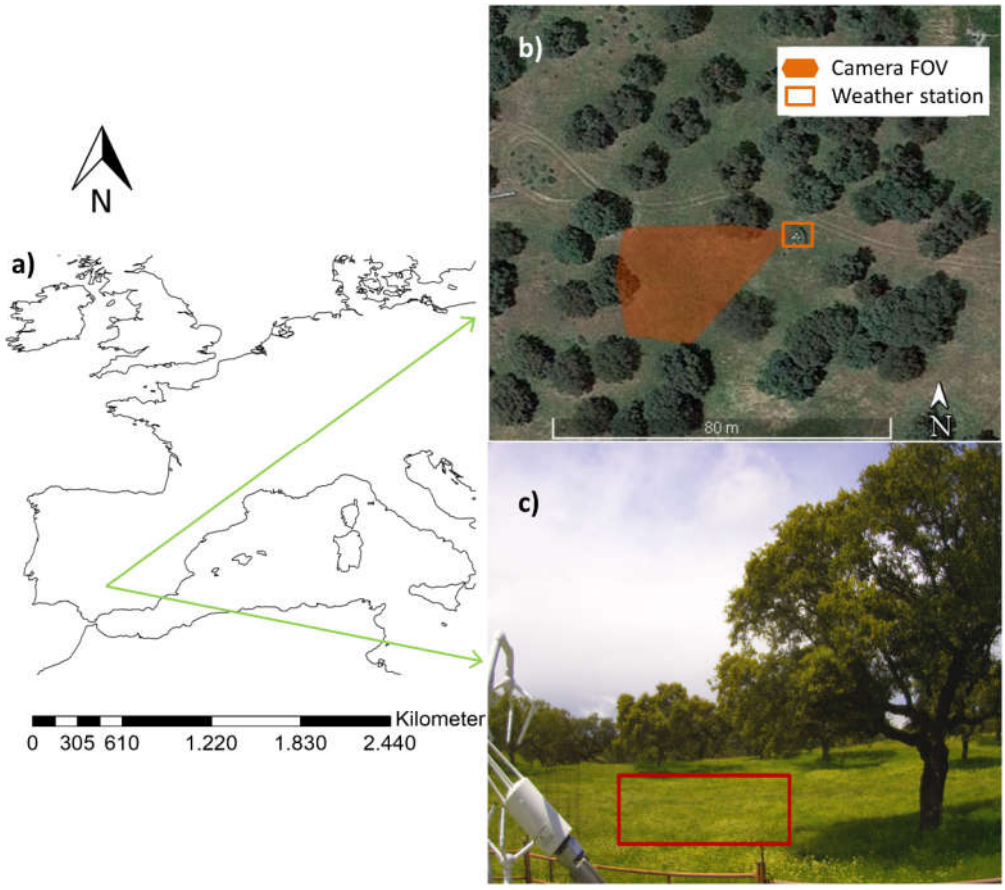

Figure 1. (**a**) Farm location. (**b**) Aerial photography of the experimental site, including the location of the weather station and the terrestrial digital camera and its field of view (FOV). (**c**) Image from the terrestrial digital camera and region of interest (ROI) for natural grass used in the analysis (red polygon).

Field measurements were taken at a grass-dominated site (Figure 1b), in which the grasses were annual species of a medium size (with a maximum plant height between 0.5–1 m) and a variable coverage. The field has a great variety of species, chiefly grams such as *Vulpia spp*, *Bromus spp* or *Aegilops spp*, although legumes such as *Trifolium spp*, *Ornithopus spp*, *Uncaria spp* or *Medicago spp* arealso found[42]. The soil at the site is dominated by Eutric Cambisols, with a loamy sand texture in the grass root zone (0–30 cm). The soil moisture content, modeled at field capacity (FC) and wilting point (WP) [43], was equal to 0.18 and 0.08 m^3/m^3, respectively.

The site's instrumentation included a digital camera, micrometeorological equipment and soil moisture probes. Terrestrial photography was acquired using a CC5MPX Digital Camera (Campbell Sci. Inc) installed at a height of 1.65 m above the ground surface. This is a programmable camera of 5 megapixels which has been specially prepared to be placed outdoors (at a thermal amplitude –40 to 60 °C). Its field of view (FOV) is 790 square meters (Figure 1b), and images were obtained from the installation every hour over the daylight period, generally from 8 a.m. to 6 p.m., from the beginning of December 2017 to the end of May 2019.

According to data availability, two study periods were defined: a first period, herein called A, from December 2017 to May 2019, with available terrestrial images on a daily basis measuring field grassland greenness, and an extended period of analysis (study period B), from July 2015 to May 2019, which covered the whole period with Sentinel-2 availability (since first acquisition time).

The set of abiotic variables measured at the site during the whole study period (Figure 1b) included the following:

1. Air temperature, recorded using an HMP45A probe (Vaisala OyJ); daily minimum (T_{min}), maximum (T_{max}) and mean temperature (T_{med}) values were computed from half-hourly records.
2. Incoming and outgoing solar radiation (Rad), measured with a four-way radiometer NR-01 (Campbell Sci. Inc); daily cumulative radiation fluxes were computed from half-hourly records.
3. Vapor pressure deficit (VPD) was derived from atmospheric pressure and relative humidity (HMP45A probe (Vaisala OyJ); daily values were computed from half-hourly records.
4. Precipitation (R) was measured with a weighing-type recording rain-gauge ARG100 (Campbell Sci. Inc); daily values were computed from the aggregation of 30 min cumulative values.
5. Volumetric soil moisture (SM) was measured at two depths (10 and 30 cm) with an ENVIROSCAN (Campbell Sci. Inc) probe at 10 min intervals. Daily values were computed from these data and averaged between both depths.

Figure 2 shows the general meteorological characterization of the study period with monthly values of R and T_{med} and the monthly average of the province of Córdoba with historical data from 1971–2000 [44]. A very irregular annual distribution of rainfall was observed, as expected, as well as a great thermal amplitude on different time scales. Compared with the historical values, the four hydrological years of the study period could be considered within the average regime in terms of mean temperature, with values in summer close to 30 °C that may drop below 10 °C in winter, and mean annual temperature of 16 °C. In terms of total precipitation, the historical annual value in the area was about 650 mm: 2015/2016 and 2016/2017 were normal periods (close to 700 mm) but with different temporal distributions; 2017/2018 was an anomalous year in the seasonal distribution of precipitation in that it was drier than average until the month of March, in which 356 mm of the final 820 mm of annual precipitation was concentrated; and 2018/2019 was the driest period (500 mm).

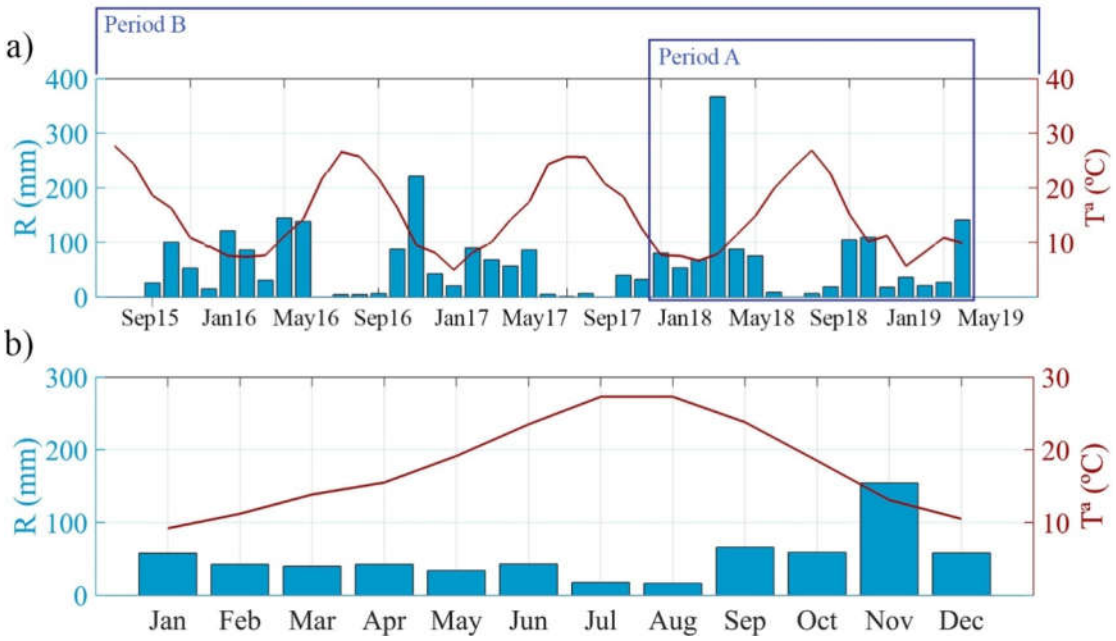

Figure 2. Monthly values of precipitation and average temperature (**a**) during study period B from the weather station in Santa Clotilde, (**b**) from historic data 1971–2000 in Córdoba.

The satellite image dataset consisted of 242 granules of Sentinel-2 images. It included all available images with less than 15% of cloud coverage from July 2015 to May 2019. From March 2017 to May 2019, the atmospherically corrected product Level 2A available from ESA (European Space Agency) was used. From July 2015 to March 2017, the images were atmospherically corrected using the module Sen2cor included in SNAP (*ESA Sentinel Application Platform v2.3.0*). Seven bands were processed to compute the different vegetation indices used in this study (the central wavelength and the bandwidth are indicated in parentheses): B2 = blue (492 nm; 66 nm), B3 = green (559 nm; 36 nm)), B4 = red (665 nm; 31 nm), B5 = red edge 1 (704 nm; 15 nm), B6 = red edge 2 (740 nm; 15 nm), B7 = red edge 3 (783 nm; 20 nm) and B8 = near infrared (NIR) (833 nm; 106 nm).

2.2. Phenological Parameters From Terrestrial Photography

The greenness of the grass, observed by terrestrial photography, was used as a field indicator of grass phenology and used to evaluate the phenological parameters retrieved from the satellite images. A quantitative value of this greenness was computed using the Green Chromatic Coordinate (GCC) (Equation 1) [45]. The GCC index is not a direct measurement of chlorophyll content, and previous research [35,46,47] has addressed its sensibility to changing levels of green pigmentation in vegetation and how canopy phenology can be monitored and quantified without the need for a human observer. This index is a non-linear transformation of the digital levels of the green color of the picture, and it is known to minimize the effects of different lighting between images taken on different days. Their characterization of greenness has proved to be better than those of other camera indices [48]:

$$GCC = \frac{G}{R + G + B} \quad (1)$$

where

GCC: Green Chromatic Coordinate index;
R: digital level in red;
G: digital level in green;
B: digital level in blue.

This index was calculated as the average value of the pixels of a homogeneous grass region of interest (ROI) (Figure 1c). Daily index values were computed for period A (December 2017 to May 2019) using the 90th percentile, in which all the GCC values were used in a 3-day moving window, assigning the average value to the central day. This methodology is assumed to reduce the error in the estimates by more than 30% [49].

To calculate the phenological parameters from GCC values, the 50% amplitude method [50] was used. In this method, the temporal evolution of a variable is considered as a function, and the state changes are supposed to be within 50% of the amplitude of this function. The amplitude was fixed for each annual growing cycle as the difference of the minimum GCC (baseline value) and the maximum value (peak value). The parameters calculated were as follows:

Start of season (SOS): time when 50% of the amplitude is reached.

Peak of season (POS): time when the data reach the maximum value of the cycle.

End of season (EOS): time when 50% of the amplitude is reached to the right of the peak value.

To homogenize the extraction of values, the data were fitted using a double logistic function (Equation 2), which is commonly employed to process remotely sensed data for phenology monitoring [51–53]. This function has proved to be useful for reducing the noise in a satellite time-series and enforcing a general seasonal shape on noisy data [54].

$$v(t) = v_{min} + v_{max}\left(\frac{1}{1+e^{x1y1t}} - \frac{1}{1+e^{x2y2t}}\right)\text{v(t) = v} \quad (2)$$

where

v(t): value of the function at time t;

v_{min}: minimum value of the amplitude;

v_{max}: maximum value of the amplitude;

x and y: parameters that control the shape of the curve. x_1 and x_2 control the left and right inflexion points, respectively, and y_1 and y_2 represent the rate of change at time t.

The TIMESAT program [51,54,55] was used to fit the double logistic function to the time series and extract the phenological parameters.

2.3. Selection of Satellite Vegetation Indices

The time series of various vegetation indices, derived from Sentinel-2 images, were studied to evaluate their ability to capture the phenology of the vegetation observed in the field using terrestrial photography. An initial set of VIs, listed in Table 1, were calculated and spatially averaged in the FOV given in Figure 1b. The first group of broad-band indices included the Normalized Difference Vegetation Index (NDVI) [56], and a version of this which changed the red reflectance for the green one—the Green Normalized Difference Vegetation Index (GNDVI) [57]; the Soil Adjusted Vegetation Index (SAVI) [58]; the Enhanced Vegetation Index (EVI) [59] and a simplified version, EVI2 [60]. The new possibilities of Sentinel-2 red edge bands made a second group of narrowband indices possible, including an adaptation of the Meris Terrestrial Chlorophyll Index (MTCI) [61] and two indices developed specifically for Sentinel-2 data: the Inverted Red Edge Chlorophyll Index (IRECI) and Sentinel-2 Red Edge Position (S2REP) [25]. Finally, GCC was computed using Sentinel-2 bands and was named as GCCs to distinguish it from the GCC from the camera, herein called GCCc. All VIs were calculated for the whole study period and spatially averaged at the camera FOV.

Table 1. Vegetation indices used in the study (listed alphabetically), formulation with Sentinel-2 bands and the available spatial resolution. Bands of Sentinel-2: B2 = blue, B3 = green, B4 = red, B5 = red edge 1, B6 = red edge 2, B7 = red edge 3, B8 = near infrared (NIR). EVI: Enhanced Vegetation Index; GCC: Green Chromatic Coordinate; GNDVI: Green Normalized Difference Vegetation Index; IRECI: Inverted Red Edge Chlorophyll Index: MTCI: Meris Terrestrial Chlorophyll Index; S2REP: Sentinel-2 Red Edge Position; SAVI: Soil Adjusted Vegetation Index.

Index	Sentinel-2 Formulation	Spatial resolution
EVI	2.5(B8-B4)/(B8+6B4-7.5B2+1)	10 m
EVI2	2.5(B8-B4)/(B8+2.4B4+1)	10 m
GCCs	B3/(B2+B3+B4)	10 m
GNDVI	(B8-B3)/(B8+B3)	10 m
IRECI	(B7-B4)/(B5/B6)	20 m
MTCI	(B6-B5)/(B5-B4)	20 m
NDVI	(B8-B4)/(B8+B4)	10 m
S2REP	705+35(((B7+B4)/2)-B5)/(B6-B5))	20 m
SAVI	1.5(B8-B4)/(B8+B4+0.5)	10 m

Once the indices values were obtained for Sentinel-2 acquisition days, a daily time series for period A was computed using a linear interpolation between every two consecutive images. To minimize the effect of possible spikes due to clouds or poor atmospheric conditions, daily index values were smoothed using the Savitzky–Golay filter [62]. This method replaces each data value by a linear combination of nearby values in a moving window, helping to reduce the noise and producing a higher quality VI time series [63]. These satellite-derived time series were compared with GCCc values for the same period; the statistical analysis was able to identify those of satellite VI better on reproducing the digital camera observations. In order to compare the performance of the different indices, their values were normalized.

Similar to GCCc, satellite VI time-series were fitted to a double logistic function, and the 50% amplitude method was applied to estimate the phenological parameters, comparing their results with those obtained from GCCc data.

2.4. Selection of Abiotic Variables

The daily evolutions of different weather variables together with the water content of the root-depth soil layer were studied to locally evaluate their links with vegetation phenology and to obtain information on the main factors influencing their behavior.

The set of abiotic variables initially selected were those commonly identified in phenological studies (T_{max}, T_{med} and R), the meteorological variables often used in crop growth models (T_{min}, Rad and VPD), and the water content in the root depth of the soil layer of the grasses (SM). Daily data were obtained from half-hourly values of the weather station for the period December 2017 to May 2019, as described in section 2.1.

The relationship between these variables and the daily series of GCCc were analyzed throughout period A. The principal explanatory variable was also employed to determine phenological parameters by fitting its values to a double logistic function, as described previously, and applying the 50% amplitude method.

2.5. Satellite VI and Abiotic Variable Relationship

The dynamic of the selected satellite VI and the most significant abiotic variable were compared during period B (July 2015 to May 2019). For this purpose, data from both of them for this period were fitted to a double logistic function, and the phenological parameters were extracted in the same way as period A.

2.6. Statistical Analysis

To evaluate the relationships between the GCCc, satellite VIs, and the abiotic variables, a Pearson correlation matrix and principal component analysis (PCA) were carried out to detect the group of variables that similarly governed the behavior of the system [64]. This method generates a new set of variables, called principal components (PCs), which are linear combinations of the original ones. The variables are related by coefficients that range between −1 and 1. The closer to 1 or −1 they are in a certain PC, the higher the direct or inverse influence they exert, respectively, on the PC. All the PCs are orthogonal to each other, so there is no redundant information. Once the PCs are obtained, all the variables of the system are grouped by processes. Since the original variables have different dimensions, standardization was applied prior to the PCA by dividing each one by its standard deviation. This process was applied firstly to GCCc with satellite VIs in order to select the representative ones, and, secondly, to GCCc with the abiotic variables.

The TIMESAT program was used to fit a double logistic function to all the variables' time series and extract the phenological parameters. Finally, the coefficient of determination (R^2) and the root mean square error (RMSE) were used to evaluate the results.

All these calculations and statistical treatments were conducted by programming in MATLAB (The Mathworks Inc., MA). The algorithms used were *corcoeff* for Pearson correlation matrices, *pca* for PCA and the *Curve fitting tool* for R^2 and RMSE.

To assess the relationship between the phenological parameters estimated using the indices, the differences in days i.e., the biases with respect to the values obtained by the GCCc were computed, and the percentage of those biases was calculated with respect to the total length of the phenological cycle, with an estimated value of 210 days (seven months) as an average [1]. In the case of the joint assessment of satellite VI and the abiotic variable, the bias in days was also calculated.

3. Results

3.1. Deriving Phenological Parameters From Terrestrial Photography

Figure 3 shows the evolution of the GCCc values throughout period A consisting of one and a half growing seasons and the function fitted to those data. The days when the baseline, SOS, EOS and the two POS for the period were reached have been identified, and the pictures (Figures 3a–3e) illustrate the state of the grass at each phenological stage.

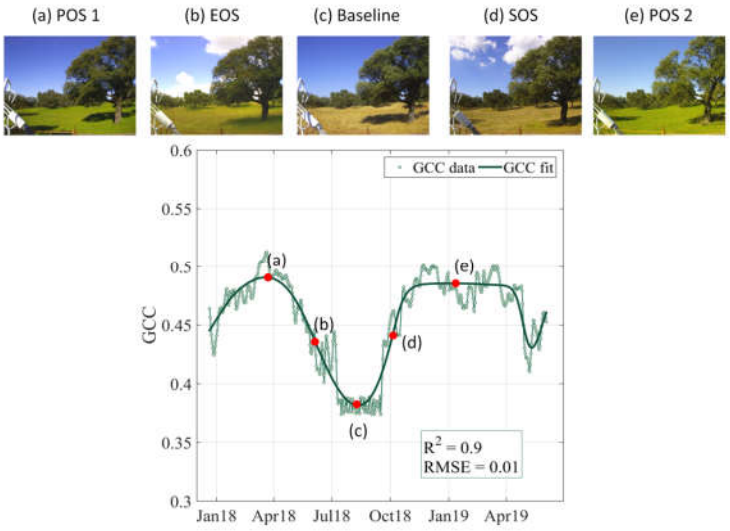

Figure 3. Evolution of GCCc (raw data, fitted function and error) throughout period A and corresponding images of the phenological dates (red dots): (**a**) peak of season (POS) 1 (03/22); (**b**) end of season (EOS (06/05); (**c**) Baseline (08/17); (**d**) start of season (SOS) (10/17); (**e**) POS 2 (01/15).

The lack of a first cycle starting point and the ending of the second one prevented the analysis of a complete single cycle. The start of the period coincided with the installation of the camera; the premature end of the second cycle was artificial and due to common farm management practices, i.e., plowing and preparing the soil for a future cereal crop. Thus, the parameters to be studied were the EOS of the first cycle, the SOS of the second and the peaks of both cycles. The baseline value used was the summer minimum of 2018.

The fitted function presented a high correlation of $R^2 = 0.9$ and a very low error of RMSE = 0.01. It can be seen that the dates of the phenological parameters given by the 50% amplitude method correctly matched the observations derived from the visual inspection of the digital camera photographs. Both POSs showed a green full cover; in the baseline, the grass was totally dry, and EOS and SOS showed the beginning of senescence and the grass becoming green, respectively.

3.2. Terrestrial Camera vs. Satellite-derived Indices

3.2.1. Satellite and Ground-based Indices Comparison

The behavior of the different satellite indices and GCCs in the study area was analyzed using the histograms of the values obtained during a complete growing cycle (year 2018). Figure 4 presents the distribution of the normalized VI values throughout this year. It can be observed that some variability was derived from the different algorithms and band combinations. All indices presented a first peak corresponding to low/very low values. This peak was more pronounced for EVI2, SAVI, IRECI and GCCs. Most indices also presented a second peak corresponding to intermediate/high index values. NDVI, EVI, GNDVI showed a more balanced distribution between both peaks than the previous group. However, MTCI and S2REP shapes do not completely follow this general pattern.

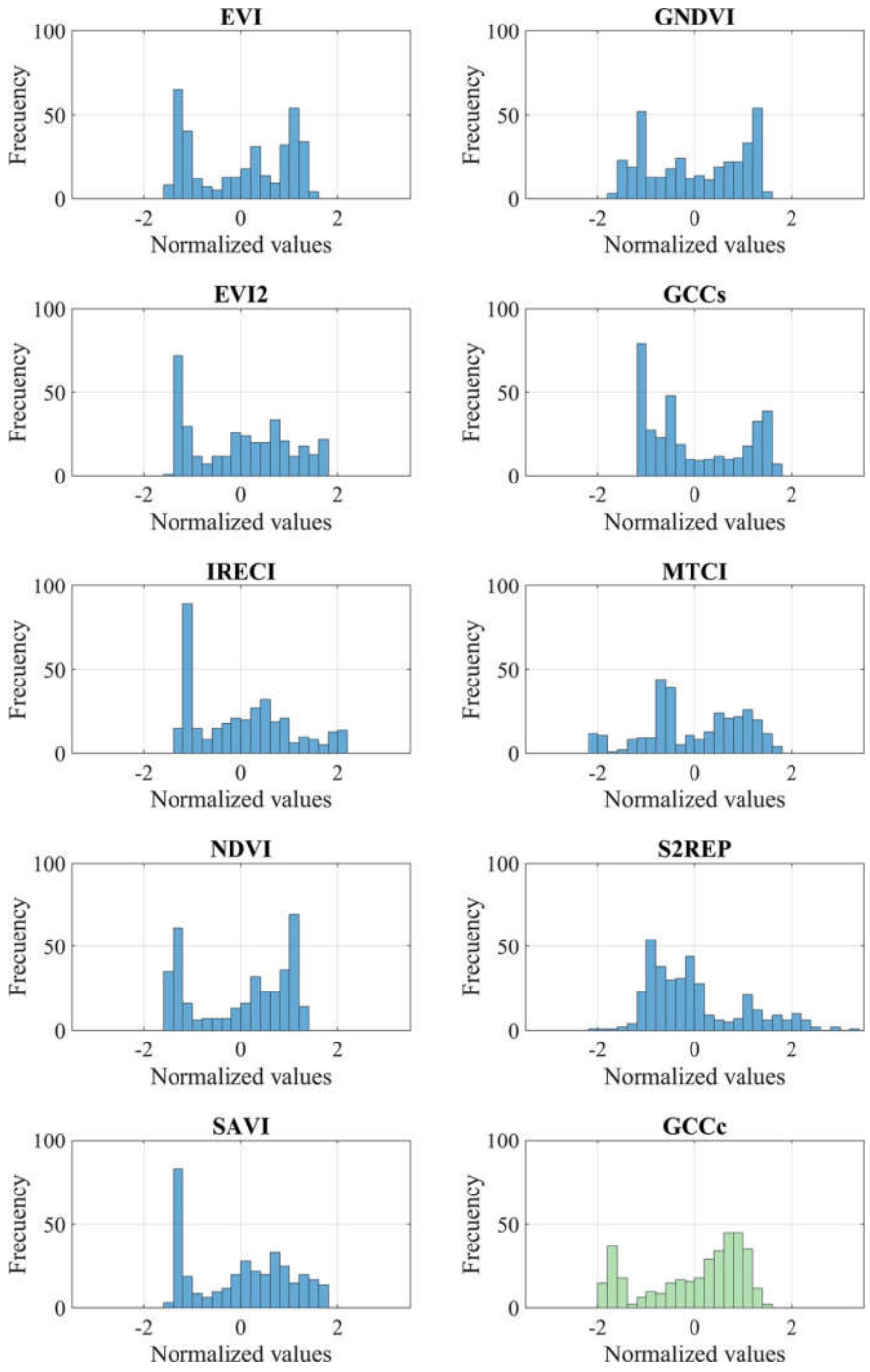

Figure 4. Histograms of vegetation index (VI) normalized values in the study area during 2018. Blue: satellite VIs; Green: Digital camera index.

Table 2 shows the Pearson correlation coefficients of daily time series of GCCc with the daily time series of a selection of satellite-derived VIs.

Table 2. Pearson correlation matrix between GCC data and the satellite VI on a daily scale. *p < 0.001.

Variable	r (GCC)
EVI	0.72*
EVI2	0.77*
GCCs	0.79*
GNDVI	0.82*
IRECI	0.71*
MTCI	0.52*
NDVI	0.83*
S2REP	–0.44*
SAVI	0.78*

The correlation of all satellite indices with GCCc was significant ($p < 0.001$) and had a high correlation value ($r > 0.7$), except for MTCI and S2REP ($r = 0.52$ and –0.44, respectively).

The results for PCA are shown in Figure 5. Most of the variance (79%) was explained by the PC 1, in which two groups of indices could be distinguished: a first group of higher coefficients (equal to or greater than 0.3) included GCCc and GCCs with the rest of the satellite indices except the MTCI and S2REP, which would together form a second group with lower or negative coefficients. In turn, these two indices presented higher values (> 0.5) in PC 2, which explained 11% of the total variance.

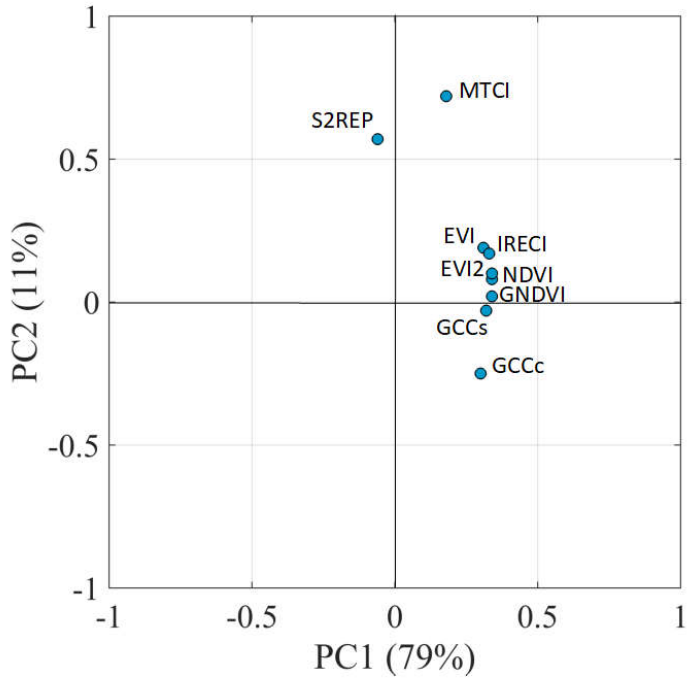

Figure 5. Principal component analysis (PCA) of GCCc and vegetation indices. The two first principal components (PCs) are shown. Between parenthesis: percentage of variance explained.

3.2.2. Satellite-derived Phenology

Based on the results of the previous section, VIs with a correlation higher than 0.7 and placed in the same group of data in PCA were selected for the subsequent analysis. Thus, seven satellite VIs were selected for the phenological analysis: EVI, EVI2, GCCs, GNDVI, IRECI, NDVI, and SAVI.

The smoothed daily data from the fitted functions are shown in Figure 6 together with the phenological parameters obtained from those VIs.

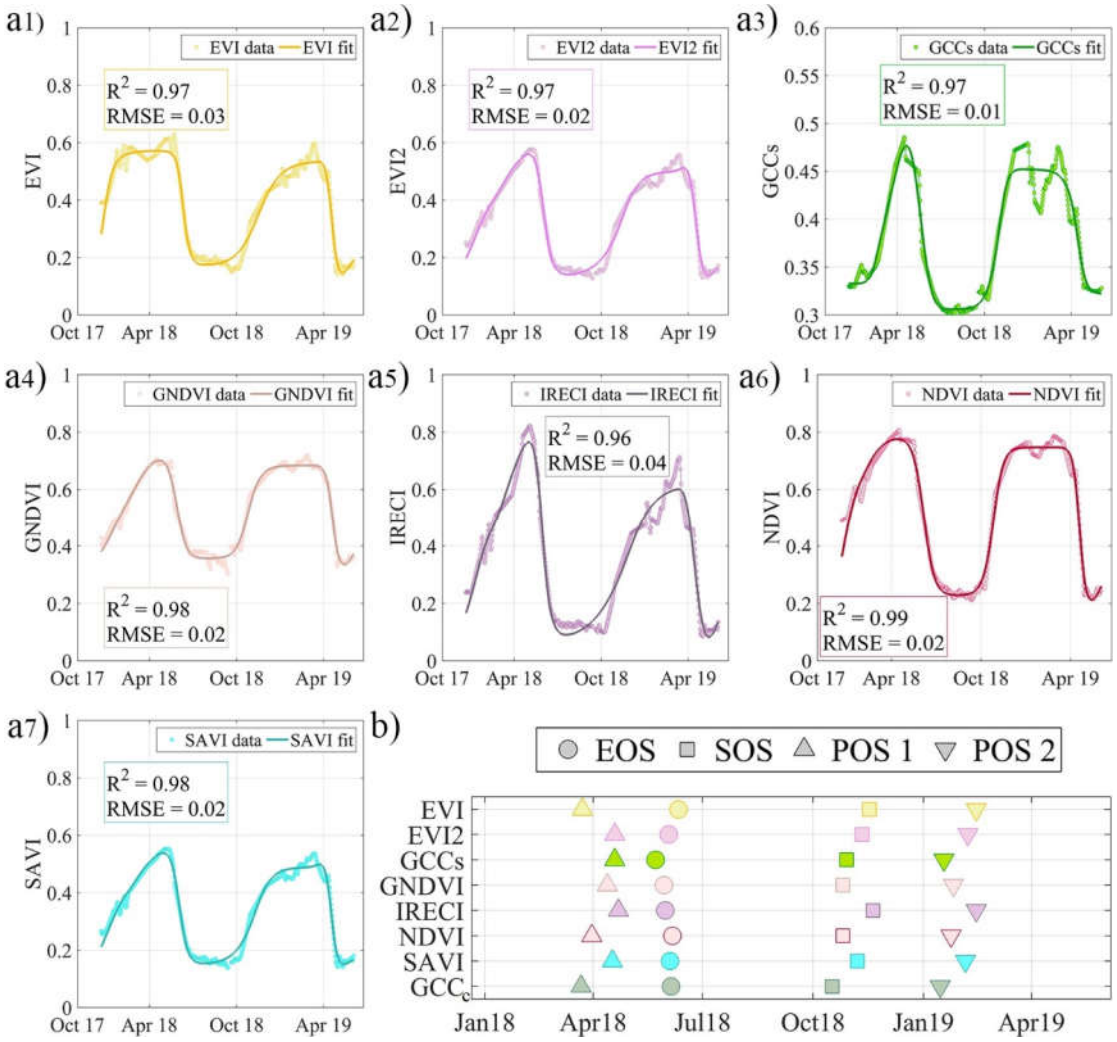

Figure 6. (**a**) Evolution of vegetation indices (raw data, fitted function and error) throughout the study period (a1 = EVI, a2 = EVI2, a3 = GCCs, a4 = GNDVI, a5 = IRECI, a6 = NDVI, a7 = SAVI). (**b**) Comparison of the phenological dates of GCCc and satellite VIs in period A.

All fitted functions showed very high correlation values ($R^2 > 0.95$) and low RMSEs (<0.03).

It can be observed (Figure 6) that the EOS was the parameter which was most similarly estimated by all indices and had the lowest bias with respect to the GCCc. The estimation of both POSs presented a higher dispersion. For this reason, POS 1 and POS 2 derived from the original raw data have been also included in Table 3 in addition to the values derived from the adjusted functions. These data are not presented for the EOS and SOS parameters due to the observed existence of erratic spikes that may cause erroneous estimations of green-up or real senescence shifts. Table 3 summarizes the biases of the phenological dates of the satellite VI with respect to GCCc (Figure 6b).

Table 3. Biases in days of the phenological parameters extracted from satellite vegetation indices with respect to GCCc, for POS 1, EOS, SOS and POS 2. The percentage of error with respect to the whole cycle is displayed in parentheses.

	POS 1 (raw data)	POS 1	EOS	SOS	POS 2	POS 2 (raw data)
EVI	–8 (3.7)	1 (0.5)	6 (2.9)	31 (14.8)	30 (14.3)	36 (17.2)
EVI2	20 (9.3)	28 (13.3)	–2 (9)	25 (11.9)	23 (11)	23 (11)
GCCs	18 (8.7)	28 (13.3)	–13 (6.2)	12 (5.7)	3 (1.4)	–3 (1.4)
GNDVI	13 (6)	22 (10.5)	–6 (2.9)	9 (4.3)	11 (5.2)	6 (2.9)
IRECI	26 (12.4)	31 (14.8)	–5 (2.4)	34 (16.2)	30 (14.3)	37 (17.7)
NDVI	4 (1.9)	9 (4.3)	1 (0.5)	9 (4.3)	9 (4.3)	2 (0.9)
SAVI	17 (8.2)	26 (12.4)	–1 (0.5)	21 (10)	21 (10)	23 (11)

The estimation of the green up (SOS) was delayed by all satellite VIs, with GCCs, GNDVI and NDVI presenting the lowest errors of around ten days (less than 10% of the cycle). The agreement was higher for the end of the season, with errors below 10% in all cases and biases of only one day using NDVI and SAVI. For both peaks of the season, there was a general delay in the estimations, with lower errors in POS 1 than in POS 2 in most cases. EVI and NDVI produced the best results for POS1, and GCCs and NDVI for POS 2. However, in the case of POS, the dates obtained using the original raw data generally improved the estimates. It could be of interest to evaluate the impact of specific weather events. In general, NDVI obtained the most consistent results and lowest errors; considering this, NDVI was selected for further analysis in this work.

3.3. Analysis of Abiotic Variables and Greenness Dynamics

The results of the Pearson correlation matrix between the daily time series of GCCc and the daily time series of selected abiotic variables for period A are shown in Table 4. All correlations were significant ($p<0.001$), and soil moisture (SM) presented the highest correlation ($r = 0.75$). Some variables, including VPD, Rad, T_{min}, T_{med}, and T_{max}, were inversely correlated with greenness. Rainfall, although positively correlated, presented the lowest coefficient of all analyzed variables. In the PCA results (Figure 7), the first PC explained 60% of the total variance, showing high coefficients (greater than 0.3) for most variables. Similar to the correlation matrix results, a first group with negative coefficients included GCCc and variables favoring an increase of soil water content (SM and R); a second group with positive coefficients was formed by variables with high values during the summer when the grass canopy was dry.

Table 4. Pearson correlation matrix between GCCc data and the abiotic variables at a daily scale. *p < 0.001.

Variable	r (GCCc)
SM	0.75*
VPD	-0.68*
R	0.17*
Rad	–0.56*
T_{min}	–0.68*
T_{med}	–0.72*
T_{max}	–0.69*

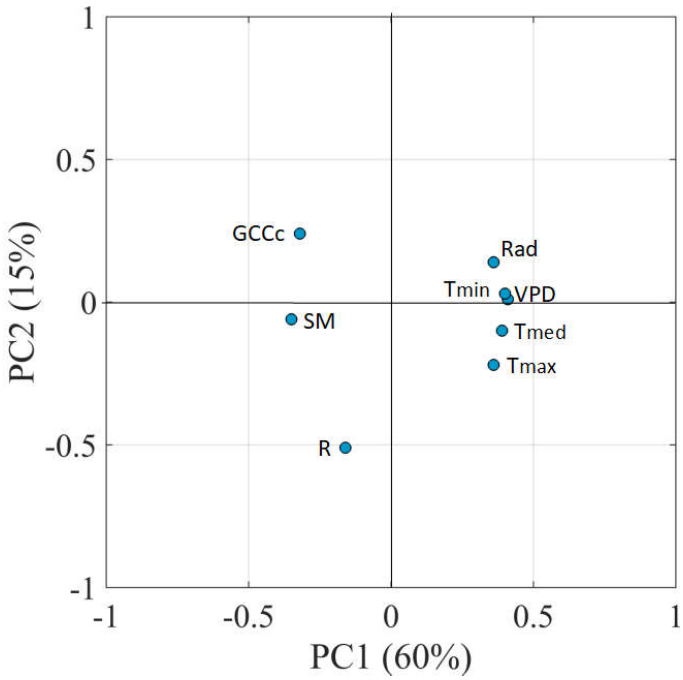

Figure 7. Principal component analysis (PCA) of GCCc and abiotic variables. The two first principal components (PCs) are shown. Between parenthesis: percentage of variance explained.

3.3.1. Grassland Phenology and Soil Moisture Relationship

Considering the previous results, SM has been selected to evaluate its capability to predict the phenology of the grass canopy of oak–grass savanna ecosystems. Figure 8a shows the distribution of SM data and the fitted function. This function presented a correlation of $R^2 = 0.9$ and an error of RMSE = 0.02, indicating a good agreement, although to a lesser extent than those obtained for GCCc and satellite VIs.

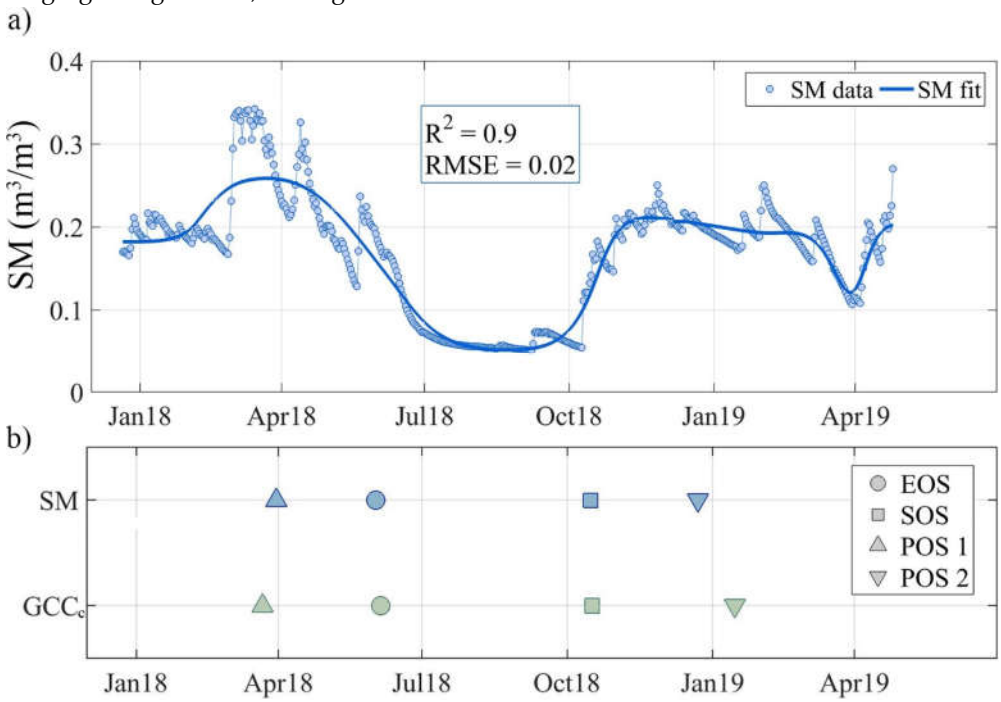

Figure 8. (**a**) Evolution of SM (raw data, fitted function and error) for the study period. (**b**) Comparison of the phenological dates of GCCc (green) and SM (blue) in period A.

The phenological parameters predicted by this function were compared to those derived from GCCc (Figure 8b). The SOS and EOS were quite similar to the timings estimated by GCCc, with a slight advance in both dates according to SM estimations. The 50% amplitude method resulted in similar values of SM, around 0.14 m^3 /m^3 on average, marking the beginning and the end of the growing season.

3.4. Relationships Between Soil Moisture and NDVI

The relationship between NDVI and SM—i.e., the variables that best suited the phenological monitoring of the grassland according to the previous results—were analyzed during period B (July 2015 to May 2019) comprising a total of four growing seasons.

Figure 9 shows the data for SM, the smoothed data for NDVI, the functions fitted to both series, and the phenological parameters extracted from them. The marked and mostly synchronized seasonality of both variables can be observed. The highest differences were found during the second year, corresponding to the growing season 2016/2017, with differences of 9 days (4.3%) for SOS, 28 days (13.3%) for POS and 16 days (7.6%) for EOS. Both fitted functions showed a high correlation (R^2 = 0.9 for SM and R^2 = 0.93 for NDVI) and low errors (RMSE = 0.02 for SM and RMSE = 0.04 for NDVI). Compared to GCCc, NDVI showed a later response to water availability, resulting in lower differences in monitoring the phenology.

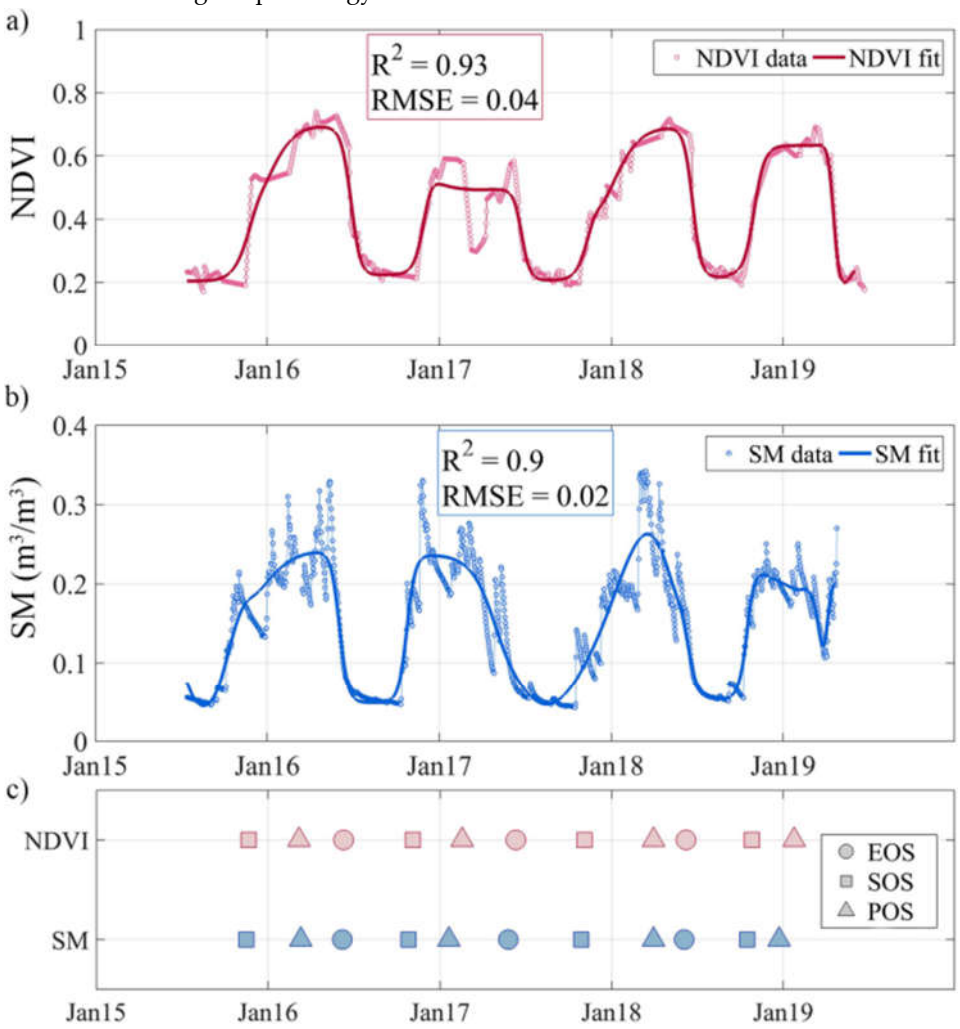

Figure 9. (**a**) Evolution of NDVI (raw data, fitted function and error) throughout the study period. (**b**) Evolution of SM (raw data, fitted function and error) during the study period. (**c**) Comparison of the phenological dates of NDVI and SM in the whole study period

4. Discussion

4.1. Capability of the Terrestrial Photography to Provide Phenological Parameters

The two hydrological years of study period A are an example of Mediterranean climate variability (Figure 2), and therefore of phenology variability. In 2017/2018, most of the precipitation was concentrated in a short period of time at the beginning of March, and POS 1 occurred shortly after those intense events. On the other hand, 2018/2019 was a drier year, but with a more regular rainfall distribution in the fall and spring. A lower GCCc maximum value was reached, but the growing season was longer, producing a plateau shape in which an intermediate value was identified as POS 2.

GCCc values ranged between 0.35 and 0.5, reaching their maximum values between November and April, eventually presenting drops of varying duration and intensity due to the particular weather conditions of the year. This temporal trend of the GCCc time series was similar to the one observed by other studies in Mediterranean grasslands [65,66]. The reasonable behavior of the CGGc of canopy status in the field according to the weather conditions, the previous studies and the visual observations provided by the terrestrial photography supported the use of GCCc time series as a reference to evaluate the performance of satellite vegetation indices.

4.2. Comparison of Ground and Satellite-based Indices

The first peak with a low value observed in Figure 4 corresponds to a predominance of dry grass/bare soil coverage during the dry season. Indices particularly sensitive to soil contribution, such as EVI, EVI2 and SAVI [58], present a higher concentration around these low values. The second peak may correspond to the central time of the spring, when the greening is widespread, while intermediate values reflect periods of green-up and senescence. The narrow band indices (IRECI, MTCI and S2REP) showed a wider distribution in values, probably due to the greater sensitivity to the changes that the red edge presented. It is worth mentioning that NDVI and GNDVI presented a sharpened ending at high values compared to other indices, with an accumulation of intermediate–high values that did not reach its maximum. This might indicate a certain degree of saturation of both indices under high grass cover conditions. This issue, described in previous studies for forest or high biomass crops [67,68], appears to occur here also to some extent. It is also worth noting the difference in the distribution of GCCs and GCCc; with the same formulation, the satellite version presented lower values than those calculated using the field camera. This result could have been due to the differing geometry of the image acquisition.

The low correlation for MTCI shown in Table 2 could be explained by the rapid response of this index to chlorophyll variations [61]. This causes the time series to follow a different trend than the rest of the indices, which is more connected to green foliage density [69] with smoother transitions. MTCI has presented good results in more homogeneous canopies, such as subalpine grasslands [33] or in deciduous trees in Central Europe [70]. In this case, the high diversity of species, typical of Mediterranean grasslands, might explain the high variability observed in these values. The case of S2REP is similar since it was also designed to measure chlorophyll variation using three bands located in the red-edge region, and allegedly provides a better characterization of the red-edge slope than MTCI [25]. IRECI also uses three bands in the red edge, although the high correlation presented with GCCc might be explained by a different formulation. In this case, the index was designed to focus on the chlorophyll content of the canopy instead of the leaf scale addressed by S2REP [25]. The influence of the vegetation ground coverage and foliage density was higher and more similar to the other broad-band indices.

The results for PCA in Figure 5 showed that most of the variance (79%) was explained by the PC 1, in which two groups could be distinguished; a first group of higher coefficients (equal to or greater than 0.3) included GCCc and the rest of the satellite indices except the MTCI and S2REP, which would form a second group with lower or negative coefficients. In turn, these two indices had high values (>0.5) in PC 2, which explained 11% of the total variance. This grouping confirmed the results obtained by the Pearson correlation and suggested that these two red-edge indices might be related

to a different process than the rest. In that case, MTCI and S2REP would be more useful for estimating leaf chlorophyll content [61,71], while the rest were more influenced by canopy foliage. Regarding the pixel size, it does not seem to have had an influence on previous results or to determine the selection of the index for the conditions of this study. IRECI, at 20 m in size (like MTCI and S2REP), was included in the subsequent phenological analysis.

The estimation of the green up (SOS) was delayed by all satellite VIs, but GCCs, GNDVI and NDVI presented low errors of around ten days (less than 10% of the cycle). The agreement was higher for EOS, with errors below 10% in all cases and biases of only one day using NDVI and SAVI. However, in the case of POS, the dates obtained using the original raw data generally improved the estimates—something of interest to evaluate the impact of specific weather events—nevertheless, in the case of analyzing long time series, fitted functions provide a useful homogenization procedure, generally leading to a more consistent analysis.

The disagreement in terms of POS estimations between satellite-borne and ground-borne sensors can be explained by the different acquisition angle of both systems. The field camera captures flowering and the presence of non-photosynthetic elements such as stems [46], which might reduce greenness and anticipate peak time. Despite this factor, NDVI exhibited a very similar behavior to GCCc, with lower differences in days than those of previous studies in grasslands [66,72]. A possible reason for the comparatively lower errors could be the higher spatial resolution employed in this case (10 m for Sentinel-2 versus 250 or 500 m for MODIS, as previously used). This factor may become a major issue in mixed grass/tree systems [34]. GNDVI also provided good general results for EOS and SOS, although POS, especially for the first year, was somewhat delayed. GCCs, with the same formulation as GCCc, presented higher errors than NDVI when applied to satellite bands. EVI, EVI2, IRECI and SAVI displayed the highest difference of days in this study, despite EVI2 and NDVI having performed similarly in other types of grasslands [47] and with even better EVI2 results for maize yield [73] and EVI for deciduous tree coverages ([74,75]). In general, NDVI obtained the most consistent results and the lowest errors (less than 10% in all cases). These good results support the use of this multi-scale approach to complement phenology studies in grasslands. Even though the availability of terrestrial camera observations is not widespread, the increasing number of these stations is a promising framework to encourage this combined strategy.

4.3. Analysis of the Dynamics of Abiotic Variables, Greenness and Phenology

The results shown in Table 4 are consistent with the water-limited condition of this ecosystem, where the dynamics of plant development and soil moisture are intimately related. This explains the high correlation of SM with GCCc, and the positive values found for SM and rainfall, with both variables favoring an increase in soil water content. The low correlation coefficient of the rainfall was also reasonable considering the daily time scale and the bulk analysis performed over a period with high rainfall variability. Rainfall has been previously related to the timing of leaf flush in dry forest [76], suggesting that an event-based analysis at specific times of the year might produce different results. High values of solar radiation, air temperature and VPD—characteristics of the dry season—are linked to an increase in atmospheric water demand, thus accelerating the water stress process in the vegetation and explaining the inverse relationships with grass greenness. This general description of the ecosystem behavior is also supported by PCA results (Fig 7). The first PC explained 60% of the total variance, showing high coefficients (greater than 0.3) for most variables. Similar to the correlation matrix results, a first group with negative coefficients included GCCc and variables favoring an increase in soil water content (SM and R); a second group with positive coefficients was formed by variables with high values during the summer when the grass canopy was dry. These variables might negatively influence the plant water status in water scarce conditions. No significant differences in both analyses were obtained when the different growing season stages were analyzed separately.

Analyzing the behavior of SM shown in Figure 8, the value of SM selected by the 50% method for the EOS seems slightly high, as it coincides with a fraction of around 60% of the total available soil water. This depletion fraction is close to the threshold used for crops [77] below which the soil

water can no longer be transported quickly enough towards the roots to meet the transpiration demand, and the plant starts to experience stress. However, in this application, this threshold is supposed to indicate the complete senescence of the plant rather than the beginning of plant water stress, which might indicate that both processes—the soil drying and the response of the vegetation—happened very quickly.

The use of SM to compute the POS in this environment makes less sense than for SOS and EOS, and the biases found with respect to GCCc estimations confirm this point. First of all, the data reflected a significant difference between the two POSs reached in the field-calibrating period as a consequence of the natural climatic variability of this region. POS 1 estimation with SM was closer to GCCc estimation, occurring with a bias of 9 days (4.3%). For POS 2, the bias was of –23 days (11%), presenting a difficult identification of the peak due to a flatter distribution of SM over the mid-growing season. Looking at the distribution of GCCc (Figure 3) and SM (Figure 8a), the shape of the first cycle was sharper because high SM values were concentrated in a short period, producing a fast response in GCCc values, with the POS reached before the SM peak, once the plant had no limitation to accessing soil water. In the second cycle, the distribution of SM followed a distribution with two similar low peaks (November 2018 and February 2019) with a slightly drier period around January. This reduction in SM was reflected by both GCCc (Figure 3) and some satellite VIs such as NDVI or GCCs (Figure 6), confirming the close link between SM and greenness and also the fast response of the vegetation to relatively small reductions in SM. This change in SM was small and it was not reproduced by the different fitted functions however, nevertheless, it caused a notable bias in the peak identification. Using the unfitted data for the POS, the results were similar; in POS 1, there was an advance of 9 days (4.3%), and in POS 2, this was 31 (14.7%).

4.4. Relationship Between SM and NDVI

The synchronized seasonality of both variables observed in Figure 9 has already been pointed out for other vegetation types under arid or semi-arid conditions in [78], in which the authors reported an increasing synchronization following a gradient of dry season length in a region. It is worth noting here the similar shapes of both variables following the beginning and the end of the dry periods, supporting the higher control of soil moisture on vegetation development during those periods. In general, an average delay between 3 and 10 days can be noted in the estimation of most phenological parameters with NDVI with respect to SM. The highest differences were found in the second year, corresponding to the growing season 2016/2017, with differences of 9 days (4.3%) for SOS, 28 days (13.3%) for POS and 16 days (7.6%) for EOS. During that year, the grassland was plowed and sown in the middle of February, following a management practice conducted every nine years or so that is currently disappearing in the area. Therefore, these two grass-growing cycles were artificially shaped and were not adequately reproduced by the fitting function. The poor adjustment of the function affects the phenological estimations, increasing their errors. Apart from this specific case, both fitted functions showed a high correlation ($R^2 = 0.9$ for SM and $R^2 = 0.93$ for NDVI) and low errors (RMSE = 0.02 for SM and RMSE = 0.04 for NDVI). Compared to GCCc, NDVI showed a later response to water availability, resulting in lower differences in monitoring the phenology. However, this difference could simply be due to the lower temporal resolution of satellite data, with a minimum of 5 days, compared to the daily availability of the terrestrial photography.

5. Conclusions

The phenology of a semi-arid grassland was monitored using terrestrial photography, satellite images, and abiotic ground measurements. The similarities and discrepancies observed using these datasets supported the capability of satellite vegetation indices to track important phenological parameters of this canopy and highlight the close relationship between these phenological parameters and the soil moisture dynamic under the study conditions.

The methodology to process the ground and satellite time series and extract the phenological information, implemented in TIMESAT, successfully fitted the data, with high correlation coefficients and low errors ($R^2 > 0.9$ and RMSE < 0.03 in all cases at the two scales), and identified key seasonal

changes of the natural grasslands. On the ground, daily time series of the GCCc, computed using digital photography, estimated grassland phenological parameters in accordance with visual inspection and with the observed climatic conditions of the experimental study period. On the S2 satellite platform, NDVI was the index that better reproduced ground GCCc behavior, with the highest correlation (r = 0.83) and less than 10 days of difference for all the phenological parameters studied (representing less than 5% error within a grass cycle). None of the VIs using bands in the red-edge region improved the NDVI results. Two of them, MTCI and S2REP, followed a different trend than the rest of the explored indices. Both indices presented a high temporal variability, which could be explained by chlorophyll content variations caused by the diversity of species of this grassland, different to the more homogeneous canopies of previous studies [33,70]. The rest of the indices were more related to foliage density [69] and presented smoother changes in this canopy.

The abiotic variable that best represented the behavior of GCCc was SM (r = 0.75). The estimation of SOS and EOS phenological parameters using SM time series presented a good agreement with GCCc, with SM reaching threshold values a few days before greenness ones, as measured by GCCc. The values of SM found at the beginning and the end of the growing seasons, when changes between green and senescent stages occurred, were high according to the modeled soil water holding capacity. This might indicate that these modeled values were not accurate enough to assess the quick response of this canopy to the soil drying process. On the other hand, SM was not a good indicator of the POS, presenting significant biases with respect to GCCc estimations.

Finally, the behavior of NDVI and SM during the four growing seasons points out the synchronized seasonality shown in this system by the vegetation greenness, measured here by the NDVI and the SM. Higher agreement was found at the beginning and the end of the dry season, with stage changes estimated first by SM followed by NDVI with a delay of between 3 to 10 days. Taking into account these results, it is possible to monitor the water state of the soil from the phenological parameters obtained with NDVI of S2 and also to determine the phenological state of the cover from the SM with errors below ten days for this type of coverage.

Author Contributions: Conceptualization, P.J.G.-G. and M.P.G.-D.; methodology, P.J. G.-G., M.P.G.-D., M.J.P.-P. and M.J.P.; software, P.J.G.-G. and M.J.P.-P.; data curation, P.J.G.-G.; writing, review, and editing, P.J. G.-G., M.P.G.-D., M.J.P.-P. and M.J.P.; graphical deployment, P.J.G.-G. and M.J.P.-P.; supervision, M.P.G.-D. and M.J.P. All authors have read and agreed to the published version of the manuscript.

Funding: This work was supported by the SensDehesa (PP.PEI.IDF201601.16) project, co-funded at 80% by the European Regional Development Fund (ERDF), as part of the Andalusian operational program 2014–2020; additional support was provided by the project "Control and early warning of critical ecohydrological states in areas of Dehesa and high mountains through terrestrial photography", funded by the Biodiversity Foundation, Spanish Ministry of Agriculture, Fisheries, Food, and Environment.

Acknowledgments: The authors are grateful to the owner of the Santa Clotilde farm for providing access to the site.

Conflicts of Interest: The authors declare no conflicts of interest. The funders had no role in the design of the study; in the collection, analyses, or interpretation of data; in the writing of the manuscript, or in the decision to publish the results.

References

1. Olea, L., & Miguel-ayanz, A.S.. *The Spanish dehesa, a traditional Mediterranean silvopastoral system*. 21st General Meeting of the European Grassland Federation, Badajoz, Spain, 3-6 April **2006**, 1–15.
2. Scholes, R.J., & Archer, S.R.. *Tree-Grass Interactions in Savannas.* Annu. Rev. Ecol. Syst.**1997**, 28(1), 517–544. https://doi.org/10.1146/annurev.ecolsys.28.1.517.
3. Eagleson, P.S., & Segarra, R.I.. *Water-Limited Equilibrium of Savanna Vegetation Systems*. Water Resour. Res **1985** , 21(10), 1483–1493. https://doi.org/10.1029/WR021i010p01483
4. Eagleson, P.S., & Tellers, T.E.. *Ecological optimality in water-limited natural soil-vegetation systems: 2. Tests and applications.* Water Resour. Res **1982**, 18(2), 341–354. https://doi.org/10.1029/WR018i002p00341
5. Moreno, G., Gonzalez-Bornay, G., Pulido, F., Lopez-Diaz, M.L., Bertomeu, M., Juárez, E., & Diaz, M. *Exploring the causes of high biodiversity of Iberian dehesas: The importance of wood pastures and marginal habitats*. Agrofor. Syst. **2016**, 90(1), 87–105. https://doi.org/10.1007/s10457-015-9817-7.

6. Turner, N.C. *Drought resistance and adaptation to water deficits in crop plants*. Stress Physiology in Crop Plants.,**1979**, 343–372. Retrieved from https://ci.nii.ac.jp/naid/10006285376/en/.
7. Parmesan, C., & Yohe, G. *A globally coherent fingerprint of climate change impacts across natural systems.* Nature **2003,** 37–42. https://doi.org/10.1038/nature01286.
8. IPCC 2001: *Climate change 2001: Impacts, adaptation, and vulnerability. Contribution of Working Group II to the third assessment report of the Intergovernmental Panel on Climate Change (IPCC).* In Choice Reviews Online (Vol. 39). https://doi.org/10.5860/choice.39-3433.
9. Parmesan, C. *Influences of species, latitudes and methodologies on estimates of phenological response to global warming*. Glob. Change Biol, **2007**, 13(9), 1860–1872. https://doi.org/10.1111/j.1365-2486.2007.01404.x.
10. Cleland, E.E., Chuine, I., Menzel, A., Mooney, H.A., & Schwartz, M.D. *Shifting plant phenology in response to global change.* Trends Ecol. Evol., **2007**, 22(7), 357–365. https://doi.org/10.1016/J.TREE.2007.04.003.
11. Menzel, A.. *Phenology: Its importance to the global change community — An editorial comment*. Clim. Change, **2002**, *54*, 379–385, doi:10.1023/A:1016125215496.
12. Rafferty, N.E., CaraDonna, P.J., Burkle, L.A., Iller, A.M. & Bronstein,J.L. *Phenological overlap of interacting species in a changing climate: An assessment of available approaches*. Ecol. Evol, **2013**, 3 (9). https://doi.org/10.1002/ece3.668.
13. Fisher, J.I., Richardson, A.D., & Mustard, J.F.. *Phenology model from surface meteorology does not capture satellite-based greenup estimations.* Glob. Change Biol, **2007**, 13(3), 707–721. https://doi.org/10.1111/j.1365-2486.2006.01311.x.
14. Justice, C.O., Townshend, J.R.G., Holben, A.N., & Tucker, C.J. *Analysis of the phenology of global vegetation using meteorological satellite data*. Int. J. Remote Sens, **1985**, 6(8), 1271–1318. https://doi.org/10.1080/01431168508948281.
15. Reed, B.C., Brown, J.F., VanderZee, D., Loveland, T.R., Merchant, J.W., & Ohlen, D.O.. *Measuring phenological variability from satellite imagery*. J Veg Sci., **1994**, 5(5), 703–714. https://doi.org/10.2307/3235884.
16. Jin, Z., Zhuang, Q., He, J.S., Luo, T. & Shi, Y., 2013. *Phenology shift from 1989 to 2008 on the Tibetan Plateau: An analysis with a process-based soil physical model and remote sensing data*. Clim. Change, **2013**, vol. 119(2), pages 435-449, doi:10.1007/s10584-013-0722-7.
17. Viña, A., Gitelson, A.A., Rundquist, D.C., Keydan, G., Leavitt, B., & Schepers, J. *Monitoring maize (Zea mays L.) phenology with remote sensing*. Agron, J., **2004**, 96(4), 1139–1147. https://doi.org/10.2134/agronj2004.1139.
18. Xiao, X., Hagen, S., Zhang, Q., Keller, M., & Moore, B. *Detecting leaf phenology of seasonally moist tropical forests in South America with multi-temporal MODIS images*. Remote Sens. Environ. **2006**, 103(4), 465–473. https://doi.org/10.1016/j.rse.2006.04.013.
19. Duchemin, B., Hadria, R., Erraki, S., Boulet, G., Maisongrande, P., Chehbouni, A., Escadafal, R., Ezzahar, J., Hoedjes, J.C.B., Kharrou, M.H., Khabba, S., Mougenot, B., Olioso, A., Rodriguez, J.C. & Simonneaux, V. *Monitoring wheat phenology and irrigation in Central Morocco: On the use of relationships between evapotranspiration, crops coefficients, leaf area index and remotely-sensed vegetation indices.* Agric. Water Manag., **2006**, *79*, 1–27. https://doi.org/10.1016/j.agwat.2005.02.013.
20. Peña-Barragán, J.M., Ngugi, M.K., Plant, R.E. & Six, J. *Object-based crop identification using multiple vegetation indices, textural features and crop phenology*. Remote Sens. Environ., **2011**, *115*, 1301–1316. https://doi.org/10.1016/j.rse.2011.01.009.
21. Lamb, D.W., Weedon, M.M. & Bramley, R.G.V. *Using remote sensing to predict grape phenolics and colour at harvest in a Cabernet Sauvignon vineyard: Timing observations against vine phenology and optimising image resolution*. Aust J Grape Wine, **2004**, 10(1):46 – 54, doi:10.1111/j.1755-0238.2004.tb00007.x.
22. Poenaru, V., Badea, A., Dana Negula, I., & Moise, C.. *Monitoring Vegetation Phenology in the Braila Plain Using Sentinel 2 Data*. Scientific Papers. Series, E. Land Reclamation, Earth Observation & Surveying, Environmental Engineering, **2017**, VI, 175–180. Retrieved from https://scihub.copernicus.eu/.
23. Lange, M., Dechant, B., Rebmann, C., Vohland, M., Cuntz, M., & Doktor, D.. *Validating MODIS and sentinel-2 NDVI products at a temperate deciduous forest site using two independent ground-based sensors.* Sensors, **2017**, 17(8). https://doi.org/10.3390/s17081855.
24. Jönsson, P., Cai, Z., Melaas, E., Friedl, M.A., & Eklundh, L.. *A method for robust estimation of vegetation seasonality from Landsat and Sentinel-2 time series data*. Remote Sens., **2018**, 10(4). https://doi.org/10.3390/rs10040635.

25. Frampton, W.J., Dash, J., Watmough, G., & Milton, E.J.. *Evaluating the capabilities of Sentinel-2 for quantitative estimation of biophysical variables in vegetation.* ISPRS J Photogramm Remote Sens, **2013**, *82*, 83–92. https://doi.org/10.1016/j.isprsjprs.2013.04.007.
26. Richardson, A.D., Braswell, B.H., Hollinger, D.Y., Jenkins, J.P., & Ollinger, S.V. *Near-surface remote sensing of spatial and temporal variation in canopy phenology*. Ecol Appl., **2009**, 19(6), 1417–1428. https://doi.org/10.1890/08-2022.1.
27. Motohka, T., Nasahara, K.N., Oguma, H., & Tsuchida, S.. *Applicability of Green-Red Vegetation Index for remote sensing of vegetation phenology*. Remote Sens., **2010**, 2(10), 2369–2387. https://doi.org/10.3390/rs2102369.
28. Brown, T.B., Hultine, K.R., Steltzer, H., Denny, E.G., Denslow, M.W., Granados, J. & Richardson, A.D.. *Using phenocams to monitor our changing earth: Toward a global phenocam network.* Front Ecol Environ., **2016**, 14(2), 84–93. https://doi.org/10.1002/fee.1222.
29. Moore, C.E., Beringer, J., Evans, B., Hutley, L.B., & Tapper, N.J. *Tree-grass phenology information improves light use efficiency modelling of gross primary productivity for an Australian tropical savanna*. Biogeosciences, **2017**, 14(1), 111–129. https://doi.org/10.5194/bg-14-111-2017.
30. Knox, S.H., Dronova, I., Sturtevant, C., Oikawa, P.Y., Matthes, J.H., Verfaillie, J., & Baldocchi, D. *Using digital camera and Landsat imagery with eddy covariance data to model gross primary production in restored wetlands*. Agric. For. Meteorol, **2017**, 237–238. https://doi.org/10.1016/j.agrformet.2017.02.020.
31. Pimentel, R., Herrero, J., & Polo, M.J. *Subgrid parameterization of snow distribution at a Mediterranean site using terrestrial photography*. Hydrol Earth Syst Sc., **2017**, 21(2), 805–820. https://doi.org/10.5194/hess-21-805-2017.
32. Polo, M.J., Herrero, J., Pimentel, R., & Pérez-Palazón, M.J. *The Guadalfeo Monitoring Network (Sierra Nevada, Spain): 14 years of measurements to understand the complexity of snow dynamics in semiarid regions*. Earth Syst. Sci. Data, **2019**, 11(1), 393–407. https://doi.org/10.5194/essd-11-393-2019.
33. Migliavacca, M., Galvagno, M. , Cremonesec, E., Rossini, M., Meroni, M., Sonnentage, O., Cogliati, S., Mancaf, G., Diotri, F., Busetto, L., Cescatti, A., Colombo, R., Fava, F., Morra, U., Pari, E., Siniscalco, C. & Richardson ,A.D. *Using digital repeat photography and eddy covariance data to model grassland phenology and photosynthetic CO2 uptake*. Agric For Meteorol., **2011**, *151*, 1325–1337. https://doi.org/10.1016/j.agrformet.2011.05.012.
34. Liu, Z., Wu, C., Peng, D., Wang, S., Gonsamo, A., Fang, B., & Yuan, W. *Improved modeling of gross primary production from a better representation of photosynthetic components in vegetation canopy*. Agric For Meteorol., **2017**, *233*, 222–234. https://doi.org/10.1016/j.agrformet.2016.12.001.
35. Moore, C.E., Brown, T., Keenan, T.F., Duursma, R.A., Van Dijk, A.I.J.M., Beringer, J. & Liddell, M.J. *Reviews and syntheses: Australian vegetation phenology: New insights from satellite remote sensing and digital repeat photography*. Biogeosciences, **2016**, 13(17), 5085–5102. https://doi.org/10.5194/bg-13-5085-2016.
36. Norrant, C. & Douguédroit, A. *Monthly and daily precipitation trends in the Mediterranean (1950–2000)*. Theor. Appl. Climatol. **2006**, *83*, 89–106, doi:10.1007/s00704-005-0163-y.
37. Cortesi, N., González-Hidalgo, J.C., Brunetti, M., & Martin-Vide, J. *Daily precipitation concentration across Europe 1971–2010.* Nat. Hazards Earth Syst. Sci. **2012**, *12*, 2799–2810, doi:10.5194/nhess-12-2799-2012.
38. Solomon, S., Quin, D., Manning, M., Chen, Z., Marquis, M., Averyt, K., Tignort, M. & Miller, H. *Climate Change: The Physical Science Basis.* Contribution of Working Group I to the Fourth Assessment Report of the Intergovernmental Panel on Climate Change, **2017**, United Kingdom and New York, USA.
39. Kovats, R.S., Valentini, R., Bouwer, L.M., Georgopoulou, E., Jacob, D., Martin, E., Rounsevell, M. and Soussana, J.F. *Climate Change 2014: Impacts, Adaptation, and Vulnerability.* Part B: Regional Aspects. Contribution of Working Group II to the Fifth Assessment Report of the Intergovernmental Panel on Climate Change [Barros, V.R., C.B.; Field, D.J.; Dokken, M.D.; Mastrandrea, K.J.; Mach, T.E.; Bilir, M.; Chatterjee, K.L.; Ebi, Y.O.; Estrada, R.C.; Genova, B.; Girma, E.S.; Kissel, A.N.; Levy, S. MacCracken, P.R. Mastrandrea, y L.L.White (eds.)]. Cambridge University Press, Cambridge, UK and New York, NY, USA, **2014**, pp. 1267-1326.
40. Gómez-Giráldez, P.J., Aguilar, C., & Polo, M.J. *Natural vegetation covers as indicators of the soil water content in a semiarid mountainous watershed.* Ecol. Indic, **2014**, *46*, 524–535. https://doi.org/10.1016/j.ecolind.2014.06.024.
41. Andreu, A., Kustas, W.P., Polo, M.J., Carrara, A., & González-Dugo, M.P. *Modeling surface energy fluxes over a dehesa (oak savanna) ecosystem using a thermal based two-source energy balance model (TSEB) I*. Remote Sens, **2018**, 10(4), 1–27. https://doi.org/10.3390/rs10040567.

42. García-moreno, A., Fernández-Rebollo, P., Muñoz, M., & Carbonero, M.. *Gestión de los pastos en la dehesa*. Instituto de Investigación y Formación Agraria y Pesquera (IFAPA). **2016** Dep. Legal CO-614-2016. https://www.juntadeandalucia.es/agriculturaypesca/ifapa/servifapa/contenidoAlf?id=1e33ce7b-9a13-4d73-8832-f367be91c551&sector=69cc80a0-9a2d-11df-accb-b374239e8181&sectorf=69cc80a0-9a2d-11df-accb-b374239e8181&l=material.
43. Schaap, M.G., Leij, F.J., & Van Genuchten, M.T. *Rosetta: A computer program for estimating soil hydraulic parameters with hierarchical pedotransfer functions*.J. Hydrol., **2001**, 251(3–4), 163–176. https://doi.org/10.1016/S0022-1694(01)00466-8.
44. Agencial Estatal de Meteorología (Ministerio de Medio Ambiente y Medio Rural y Marino) and Instituto de Meteorologia de Portugal .*Atlas climático de España y Portugal*.**2011** ISBN: 978-84-7837-079-5 Retrieved from http://www.aemet.es/es/serviciosclimaticos/datosclimatologicos/atlas_climatico.
45. Gillespie, A.R., Kahle, A.B. & Walker, R.E.. *Color enhancement of highly correlated images. II. Channel ratio and "chromaticity" transformation techniques*. Remote Sens., **1987**, *22*, 343–365. https://doi.org/10.1016/0034-4257(87)90088-5.
46. Vrieling, A., Meroni, M., Darvishzadeh, R., Skidmore, A.K., Wang, T., Zurita-Milla, R., Oosterbeek, K., O'Connor, B. & Paganini, M. *Vegetation phenology from Sentinel-2 and field cameras for a Dutch barrier island*. Remote Sens. Environ., **2018**, *215*, 517–529. https://doi.org/10.1016/j.rse.2018.03.014.
47. Zhang, X., Jayavelu, S., Liu, L., Friedl, M.A., Henebry, G.M., Liu, Y., Schaaf, C.-B., Richardson, A.D. & Gray, J. *Evaluation of land surface phenology from VIIRS data using time series of PhenoCam imagery*. Agric. For. Meteorol, **2018**, 256–257, 137–149. https://doi.org/10.1016/j.agrformet.2018.03.003.
48. Sonnentag, O., Hufkens, K., Teshera-Sterne, C., Young, A.M., Friedl, M., Braswell, B.H., Milliman, T., O'Keefe, J. & Richardson, A.D.. *Digital repeat photography for phenological research in forest ecosystems*. Agric. For. Meteorol. **2012**, *152*, 159–177. https://doi.org/10.1016/j.agrformet.2011.09.009.
49. White, M.A., Thornton, P.E., & Running, S.W. *A continental phenology model for monitoring vegetation responses to interannual climatic variability*. Global Biogeochem Cycles, **1997**, 11(2), 217–234. https://doi.org/10.1029/97GB00330.
50. Zhang, X.Y., Friedl, M.A., Schaaf, C.B., Strahler, A.H., Hodges, J.C.F., Gao, F., Reed, B.C. & Huete, A.. *Monitoring vegetation phenology using MODIS.* Remote Sens. Environ., **2003**, *84*, 471–475. https://doi.org/10.1016/S0034-4257(02)00135-9.
51. Jönsson, P., & Eklundh, L. *TIMESAT - A program for analyzing time-series of satellite sensor data*. Comput Geoscis, **2004**, 30(8), 833–845. https://doi.org/10.1016/j.cageo.2004.05.006.
52. Fisher, J.I., Mustard, J.F. & Vadeboncoeur, M.A. *Green leaf phenology at Landsat resolution: Scaling from the field to the satellite*. Remote Sens. Environ, **2006**, *100*, 265–279.https://doi.org/10.1016/j.rse.2005.10.022.
53. Fisher, J.I. & Mustard, J.F. *Cross-Scalar Satellite Phenology from Ground, Landsat, and MODIS Data*. Remote Sens. Environ, **2007**, 109(3):261-273. https://doi.org/10.1016/j.rse.2007.01.004.
54. Eklundh, L. & Jönson, P. *TIMESAT: A Software Package for Time-Series Processing and Assessment of Vegetation Dynamics*. In: Kuenzer, C., Dech, S., Wagner, W. (eds) Remote Sensing Time Series. Remote Sensing and Digital Image Processing, **2015**, vol 22. Springer, Cham. https://doi.org/10.1007/978-3-319-15967-6_7.
55. Jönsson, P. & Eklundh, L. *Seasonality extraction by function fitting to time-series of satellite sensor data.IEEE* Trans Geosci Remote Sens, **2002**, vol. 40, 1824-1832, doi:10.1109/TGRS.2002.802519.
56. Rouse, J.W., Haas, R.H., Schell, J.A. & Deering, W.D., *Monitoring vegetation systems in the Great Plains with ERTS*. In: Third ERTS Symposium, NASA SP-351, **1973**, pp. 309–317.
57. Gitelson, A.A., Kaufman, Y.J. & Merzlyak, M.N. *Use of a green channel in remote sensing of global vegetation from EOS-MODIS*. Remote Sens. Environ., **1996**, *58*, 289–298. https://doi.org/10.1016/S0034-4257(96)00072-7.
58. Huete, A.R. *A soil-adjusted vegetation index*. Remote Sens. Environ., **1988**, *25*, 295–309. https://doi.org/10.1016/0034-4257(88)90106-X.
59. Huete, A.R., Didan, K., Miura, T., Rodriguez, E.P., Gao, X. & Ferreria, L.G. *Overview of the radiometric and biophysical performance of the MODIS vegetation indices*. Remote Sens. Environ., **2002**, *83*, 195–213. https://doi.org/10.1016/S0034-4257(02)00096-2.
60. Jiang, Z.Y., Huete, A.R., Didan, K. & Miura, T. *Development of a two-band enhanced vegetation index without a blue band*. Remote Sens. Environ., **2008**, *112*, 3833–3845. https://doi.org/10.1016/j.rse.2008.06.006.
61. Dash, J. & Curran, P.J. 2004. *The MERIS terrestrial chlorophyll index*. Int. J. Remote Sens., **2004**, *25*, 5403–5413. https://doi.org/10.1080/0143116042000274015.

62. Savitzky, A. & Golay, M.J.E. *Smoothing and Differentiation of Data by Simplified Least-Squares Procedure*s. Anal. Chem., **1964**, *36*, 1627–1639. http://dx.doi.org/10.1021/ac60214a047.
63. Chen, J., Jönson, P., Tamura, M., Gu, Z., Matsushita, B. & Eklundh, L. *A simple method for reconstructing a high-quality NDVI time-series data set based on the Savitzky–Golay filter*. Remote Sens. Environ., **2004**, 91(3-4), 332-344. https://doi.org/10.1016/j.rse.2004.03.014.
64. Jackson, J.E.. *A User's Guide to Principal Components*. John Wiley and Sons: New York, USA, **1991**, pp. 592.
65. Luo, Y., El-Madany, T.S., Filippa, G., Ma, X., Ahrens, B., Carrara, A. & Migliavacca, M.. *Using near-infrared-enabled digital repeat photography to track structural and physiological phenology in Mediterranean tree-grass ecosystems.* Remote Sens., **2018**, 10(8). https://doi.org/10.3390/rs10081293.
66. Richardson, A.D., Hufkens, K., Milliman, T., & Frolking, S. *Intercomparison of phenological transition dates derived from the PhenoCam Dataset V1.0 and MODIS satellite remote sensing*. Sci. Rep., **2018**, 8(1), 1–12. https://doi.org/10.1038/s41598-018-23804-6.
67. Huete, A.R., Liu, H.Q., & van Leeuwen, W.J.D. Use of vegetation indices in forested regions: Issues of linearity and saturation. *International Geoscience and Remote Sensing Symposium (IGARSS)*, **1997**. 4(1), 1966–1968. https://doi.org/10.1109/igarss.1997.609169.
68. Gu, Y., Wylie, B.K., Howard, D.M., Phuyal, K.P., & Ji, L. NDVI saturation adjustment: A new approach for improving cropland performance estimates in the Greater Platte River Basin, USA. *Ecological Indicators*, **2013**. *30*, 1–6. https://doi.org/10.1016/j.ecolind.2013.01.041.
69. Glenn, E.P., Huete, A.R., Nagler, P.L., & Nelson, S.G. *Relationship between remotely-sensed vegetation indices and plant physiological processes: What vegetation indices can and cannot tell us about the landscape*. Sensors, **2008**, 8(4), 2136. https://doi.org/10.3390/s8042136.
70. Rodriguez-Galiano, V.F., Dash, J., & Atkinson, P.M. *Intercomparison of satellite sensor land surface phenology and ground phenology in Europe*. Geophys. Res., **2015**, 42(7), 2253–2260. https://doi.org/10.1002/2015GL063586.
71. Sibanda, M., Mutanga, O. & Rouget, M. *Testing the capabilities of the new WorldView-3 space-borne sensor's red-edge spectral band in discriminating and mapping complex grassland management treatments*. Int. J. Remote Sens., **2017**, 38(1), 1-22. https://doi.org/10.1080/01431161.2016.1259678.
72. Browning, D.M., Karl, J.W., Morin, D., Richardson, A.D., & Tweedie, C.E. *Phenocams bridge the gap between field and satellite observations in an arid grassland ecosystem.* Remote Sens., **2017**, 9(10). https://doi.org/10.3390/rs9101071.
73. Bolton, D.K. & Friedl, M.A. *Forecasting crop yield using remotely sensed vegetation indices and crop phenology metrics*. Agric. For. Meteorol., **2007**, *173*, 74–84. https://doi.org/10.1016/j.agrformet.20.3.01.007.
74. Hufkens, K., Friedl, M., Sonnentag, O., Braswell, B.H., Milliman, T., Richardson, A.D.. *Linking near-surface and satellite remote sensing measurements of deciduous broadleaf forest phenology*. Remote Sens. Environ., **2012**, *117*, 307–321. https://doi.org/10.1016/j.rse.2011.10.006.
75. Klosterman, S.T., Hufkens, K., Gray, J.M., Melaas, E., Sonnentag, O., Lavine, I., Mitchell, L., Norman, R., Friedl, M.A. & Richardson, A.D. *Evaluating remote sensing of deciduous forest phenology at multiple spatial scales using PhenoCam imagery*. Biogeosciences, **2014** 11(16), 4305–4320. https://doi.org/10.5194/bg-11-4305-2014.
76. Jolly, W.M., & Running, S.W. *Effects of precipitation and soil water potential on drought deciduous phenology in the Kalahari.* Glob. Change Biol, **2004**, 10(3), 303–308. https://doi.org/10.1046/j.1365-2486.2003.00701.x.
77. Allen, R.G. *FAO Irrigation and Drainage Paper Crop.* Irrig. Drain., **1998**, 300(56), 300. https://doi.org/10.1016/j.eja.2010.12.001.
78. Jones, M.O., Kimball, J.S., & Nemani, R.R. *Asynchronous Amazon. forest canopy phenology indicates adaptation to both water and light availability*. Environ. Res., **2014**, 9(12). https://doi.org/10.1088/1748-9326/9/12/124021.

CONCLUSIONES

Los resultados presentados en esta tesis han demostrado la utilidad de los sensores remotos para obtener indicadores medioambientales eficaces tanto para cuantificar y apoyar el seguimiento de la vegetación y la hidrología de las zonas de estudio, como para asistir en la toma de decisiones sobre la gestión de estas zonas a escala de parcela, finca o cuenca hidrológica. Teniendo en cuenta la variabilidad del clima mediterráneo y de su vegetación, los períodos y áreas de estudio seleccionados para evaluar los distintos indicadores han recogido buena parte de esta heterogeneidad y se pueden considerar representativos de las condiciones más frecuentes en estos sistemas.

En el capítulo 2, queda mostrada la eficacia del uso del vigor de la vegetación de cubiertas naturales como indicador de las condiciones de humedad del suelo al final del año hidrológico. Las tendencias temporales y espaciales del NDVI, derivado de imágenes Landsat 5 y 7, se calcularon y se relacionaron con los diferentes patrones hidrológicos establecidos con el modelo hidrológico WiMMed. La heterogeneidad en el comportamiento hidrológico durante el período de estudio (914.5 mm de precipitación anual en el año más húmedo (2009-2010) y 284.4 mm en el más seco (2004-2005)) se reflejó en las diferencias en los valores de NDVI, más o menos constantes en coníferas (0.5-0.6) y más variables para las cubiertas de matorral. Las correlaciones entre las variables para las diferentes cubiertas y el ACP a escala espacial mostraron que, para las cubiertas de coníferas el SCWd se relacionó con las variables involucradas en el balance de agua líquida del suelo. En el caso del matorral, también se relacionó con el NDVI y las variables implicadas en la dinámica de la nieve. En la zona de encinar-matorral se produjo un comportamiento intermedio. Los mejores ajustes temporales se encontraron con ajustes exponenciales entre los valores espaciales anuales promedio de SWCd y NDVI en la cubierta de matorral con coeficientes r^2 superiores a 0,7 y valores de RMSE inferiores a 0,051. En esta cubierta también se encontraron las mayores correlaciones en el análisis intra-anual, alcanzando coeficientes r^2 superiores a 0.85 en los mejores años. Con todo ello, se puede concluir que la mejor cubierta para ser usada como indicador de la humedad del suelo al final del año hidrológico en el área de estudio es la de matorral, lo que puede ser tenido en cuenta como punto de partida para la validación de modelos hidrológicos en zonas remotas.

En el capítulo 3, se ha adaptado y aplicado un modelo LUE a los pastizales de un ecosistema dehesa a dos escalas diferentes y utilizando imágenes de dos satélites para explorar su capacidad de servir, respectivamente, como indicador de la variabilidad de la productividad de los pastizales a escala regional y para el seguimiento de la gestión a nivel local o de parcela. Los resultados mostraron precisiones admisibles en ambas escalas, de acuerdo con los objetivos del estudio, después de la calibración de los parámetros fPAR y ε_{max} teniendo en cuenta las características de los pastizales mediterráneos y el efecto del arbolado. Los errores promedio en el NPP acumulado, obtenido a escala regional durante los dos años hidrológicos analizados,

fueron del 13%. Esta precisión se considera aceptable para este tipo de cubierta, especialmente cuando se compara con los resultados utilizados y aceptados en cultivos agrícolas, con coberturas del suelo más homogéneas que estos pastizales naturales. A escala de parcela, el error en la estimación fue del 16%, también se consideró aceptable para el uso propuesto, dado que las mejoras realizadas en el pasto y evaluadas por este procedimiento pueden aumentar la producción hasta el 70%. Estos resultados respaldaron el uso de este enfoque como una herramienta para el seguimiento de los pastizales de dehesa con diferentes propósitos, como apoyo en el diseño de instrumentos de política agraria para la conservación y mejora del ecosistema; o bien para proporcionar servicios de asesoramiento a los agricultores y ganaderos para mejorar las prácticas de gestión. En este capítulo también se exploraron diferentes enfoques para la parametrización del efecto del estrés hídrico en la producción primaria bruta (GPP) en el sistema dehesa, como punto de partida para profundizar en este indicador vinculado a la producción del pasto. A escala diaria, el uso combinado de un índice de estrés hídrico además de los umbrales meteorológicos proporcionó las mejores estimaciones de GPP, especialmente para las estaciones secas (valores de r^2 alrededor de 0.8 y RMSE de 0.4). Sin embargo, este método presentó un sesgo que, en los valores acumulados, resultó en una subestimación significativa de las estimaciones estacionales. El uso de un valor fijo presentó los resultados más pobres, apoyando la necesidad de factores de atenuación ambiental.

En el capítulo 4, se estudió el vínculo entre la fenología del pasto y la dinámica del agua en el suelo utilizando una combinación de fotografía terrestre, imágenes satelitales y medidas en campo. Las similitudes y discrepancias observadas al usar este conjunto de datos respaldaron la capacidad de los índices de vegetación derivados de imágenes de satélite para obtener parámetros fenológicos relevantes para el pastizal y resaltaron la estrecha relación entre estos parámetros fenológicos y la dinámica de la humedad del suelo bajo las condiciones del estudio. Los resultados mostraron que los parámetros fenológicos estimados por el NDVI de S2 ($r = 0.83$, $p < 0.001$) y la humedad del suelo (SM) ($r = 0.75$, $p < 0.001$) presentaron la mejor relación con los derivados de las observaciones proporcionadas por la cámara digital terrestre. Finalmente, el comportamiento de NDVI y SM durante los cuatro periodos de crecimiento que se analizaron mostraron la sincronización en este sistema de la dinámica de ambas variables, con cambios de estado fenológico estimados primero por la humedad del suelo, seguido por NDVI, con un retardo de entre 3 y 10 días. Teniendo en cuenta estos resultados, es posible realizar un seguimiento del estado hídrico del suelo a partir de los parámetros fenológicos obtenidos con el NDVI de S2 y también determinar el estado fenológico de la cubierta a partir de SM con errores por debajo de diez días para este tipo de cubierta.

Estos resultados también han puesto en evidencia la necesidad de profundizar en determinados aspectos de los indicadores propuestos, con el fin de mejorar la precisión de las

estimaciones y de ampliar sus condiciones de aplicación. En concreto, se identifican los siguientes puntos para futuras líneas de investigación en este ámbito:

- En el caso primer indicador, es necesario abordar estudios en escalas de tiempo más cortas y usando cubiertas naturales con ciclos de crecimiento estacional, como sería el de pasto de alta montaña. Esto nos permitiría evaluar la efectividad de su uso para eventos de lluvia concretos y no solo para el año hidrológico completo.

- El método propuesto para eliminar la contribución de los árboles a la señal de NDVI parece adecuado en las condiciones del área estudiada. Sin embargo, la densidad de los árboles de estas áreas fue baja (<50%) y únicamente incluían un estrato herbáceo, por lo que el rendimiento de este enfoque en áreas con presencia de árboles caducifolios o un estrato de arbustivo desarrollado requeriría de un análisis más detallado. Del mismo modo, el parámetro de eficiencia en el uso de la luz también exige más atención. Algunos aspectos del mismo, como la influencia de las propiedades del suelo y la evaluación del modelo en situaciones extremas de alta y baja producción, deben abordarse en el futuro para reducir los errores actuales. Por último, el efecto del ganado no se ha tenido en cuenta en este indicador y sería de gran utilidad para evaluar el efecto de las rotaciones del ganado en la producción.

- El desarrollo de futuras aplicaciones del indicador fenología-hidrología requeriría una serie temporal más larga que la actualmente disponible de datos de Sentinel-2. Esto permitiría evaluar el efecto de años con condiciones climáticas extremas. Por otro lado, los resultados alcanzados animan a ampliar este seguimiento a una escala espacial mayor, teniendo en cuenta factores adicionales como la topografía del terreno.